Asian Journal of Chemistry; Vol. 36, No. 10 (2024), 2337-2358

ASIAN JOURNAL OF CHEMISTRY

https://doi.org/10.14233/ajchem.2024.32313

DFT, Structure Activity Relationship, Fukui, Wave Function, NBO, NLO, Spectral and Hole-Electron Analyses of Dexmethylphenidate

E. JIMLA PUSHPAM and J. WINFRED JEBARAJ*

Department of Chemistry, St. John's College (Affiliated to Manonmaniam Sundaranar University, Tirunelveli), Palayamkottai-627002, India

*Corresponding author: E-mail: winfred.chem@st.johnscollege.edu.in

Received: 15 July 2024; *Accepted*: 29 August 2024; *Published online*: 30 September 2024; AJC-21765

Dexmethylphenidate (DMP) is used to treat attention deficit hyperactivity disorder (ADHD) and belongs to the central nervous system (CNS) stimulant group of medicines. The physical properties of DMP were analyzed under the DFT/B3LYP/6-311++G(d,p) basis set. The ESP study reveals the electrophilic attack is possible, while FMO analysis shows that the molecule is hard, stable and an electron donor. The non-covalent interaction (NCI) study explains that van der Waals and steric repulsion forces are observed. The HEI studies indicated that this molecule has CT excitation in the S0→S5 state. The shaded surface map analysis reveals the presence of electron depletion regions in this molecule. The UV-Vis spectral analysis was carried out in various solvents. The Fukui function analysis conveys that 7C is the best domain for electrophilic attack. Theoretical IR determinations and NLO properties were also performed. The structure-activity relationship findings were performed in order to improve the docking score.

Keywords: Dexmethylphenidate, DFT, Structure activity relationship, Non-covalent interaction, NBO, HEI.

INTRODUCTION

Attention deficit hyperactivity disorder (ADHD) is a neuro-behavioural condition. It affects attention deficit hyperactivity in children and adolescents. It is characterized by executive dysfunction leading to excessive and widespread symptoms of hyperactivity, inattention, impulsivity and emotional deregulation, which are age-inappropriate overall and impede in a variety of circumstances [1-3]. The symptoms of ADHD are generated by executive dysfunction [4]. However, the exact reasons for ADHD are not-known. Genetic considerations are significant; 74% of cases of ADHD are heritable and tend to run in families [5]. In 2001, dexmethylphenidate received FDA approval for use in medicine and can be purchased as a generic drug. With almost 4 million prescriptions, it was classified as the 130th most often prescribed drug in the US in 2020. The symptoms of ADHD in children showed significant improvement when treated with dexmethylphenidate XR compared to a placebo [6]. This compound still requires execution in order to carry out the thorough DFT analysis. We thus aimed to understand conceptually about the stability, structural information, and other features of wave function analysis of this molecule.

Density functional theory (DFT) is a widely recognized quantum mechanical (QM) approach employed in the fields of physics and chemistry. This method determines the electronic structure of atoms, molecules and solids. When larger (and often more relevant) molecular systems are thoroughly examined, the ability to make accurate predictions becomes crucial in the electrical theory of structure [7]. In present study, the title compound, dexmethylphenidate (DMP) has been investigated. Due to its significant pharmacological role, DMP attracted our interest to investigate its structural properties in depth, including NBO, excitation studies, *etc*. The results of the NBO research will shed more light on the compound's stability.

COMPUTATIONAL METHODS

The 2D structure was drawn using the Chemsketch tool [8] and optimized with the help of the Avogadro program [9]. In order to save computing time and produce accurate results, optimization is a crucial step. The target molecule's electronic structural calculation uses the Gaussian 16W package and Gaussview 06 packages [10,11]. All the findings were performed based on DFT [12], while the Becke's three-parameter

functional (B3LYP) method with the 6-311++G(d,p) basis set was preferred for all the determinations [13]. Usually, B3LYP and DFT calculations show the significant results with experimental values [14]. The absence of imaginary frequencies verifies the thorough optimization, which was further confirmed by the GaussSum 3.0 program [15]. Parameters such as aromaticity, non-covalent interaction (NCI), aromaticity projection onto a shaded surface map, aromaticity, hole-electron interaction and surface-to-molecular (STM) analysis were also computed using the Multiwfn 3.8 tool [16], while the graphical outputs were generated using VMD 1.9.3 [17]. The potential energy distribution analysis was carried out by the VEDA4 software [18].

RESULTS AND DISCUSSION

Electronic structure: The molecular formula of dexmethylphenidate (DMP) is $C_{14}H_{19}NO_2$. Table-1 listed the details of the atom of the optimized molecule. The details about the electronic structure of the investigated molecule is presented in Table-2. The 2D and 3D of the optimized molecule with complete convergence and full optimization are presented in Fig. 1.

TABLE-1
ATOM LIST OF THE OPTIMIZED DEXMETHYLPHENIDATE

1	2	3	4	5	6
C	C	C	C	C	C
7	8	9	10	11	12
C	C	N	C	C	C
13	14	15	16	17	18
C	C	O	O	C	H
19	20	21	22	23	24
H	H	H	H	H	H
25	26	27	28	29	30
H	H	H	H	H	H
31	32	33	34	35	36
H	H	H	H	H	H

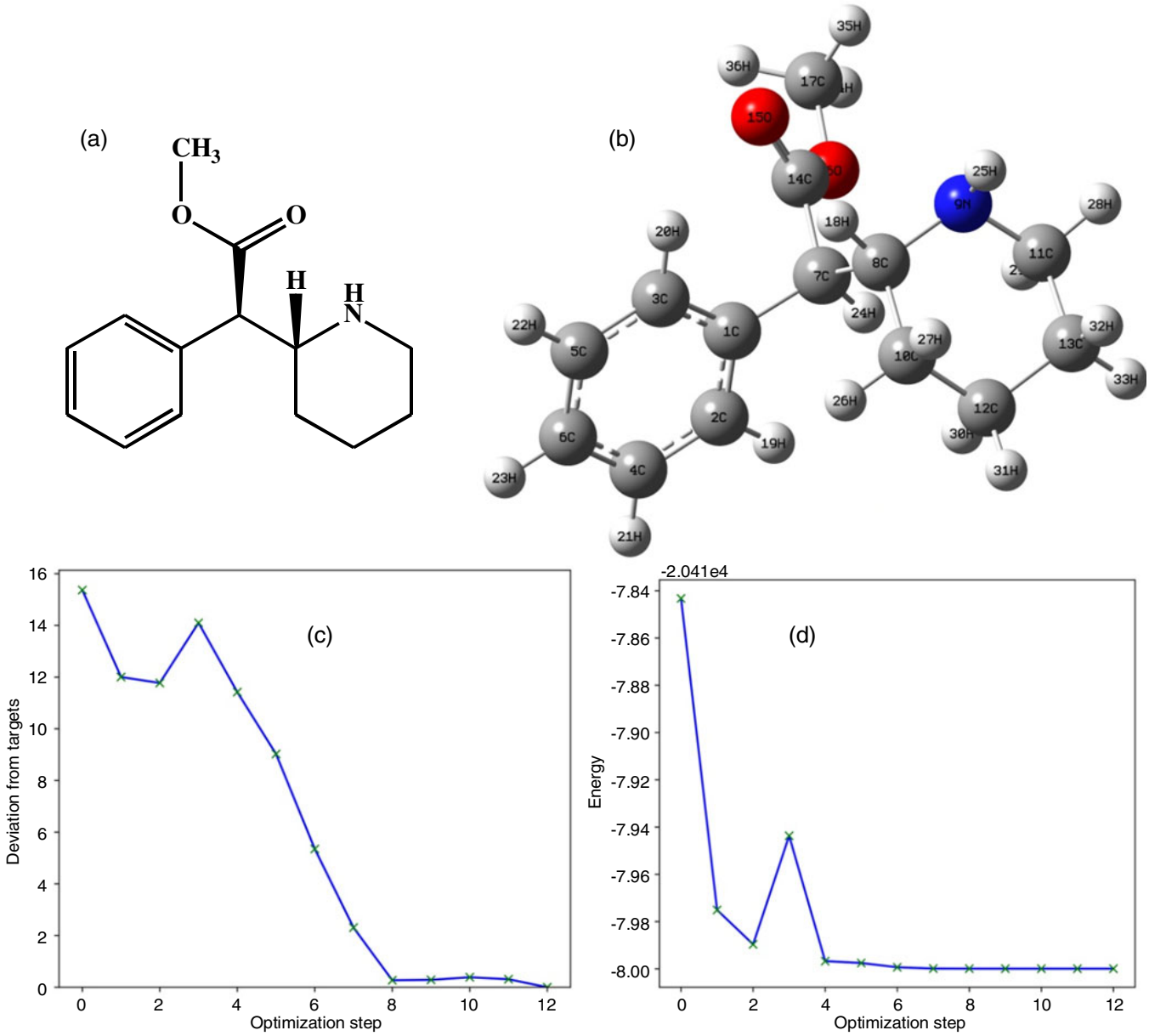

Fig. 1. (a) 2-D (b) optimized 3-D (c) complete optimization (d) full convergence images of dexmethylphenidate

TABLE-2
BOND LENGTH, BOND ANGLE AND DIHEDRAL ANGLES OF DEXMETHYLPHENIDATE MOLECULE UNDER THE DFT/B3LYP/6-311++G(d,p) BASIS SET

S. No.	Atom set	Bond distance (Å)	Atom set	Bond angle (°)	Atom set	Dihedral angle (°)	Planarity
1	1C-2C	1.399	2C-1C-3C	118.5	3C-1C-2C-4C	-0.5	–SP
2	1C-3C	1.401	2C-1C-7C	119.9	3C-1C-2C-19H	179.4	AP
3	1C-7C	1.523	3C-1C-7C	121.6	7C-1C-2C-4C	179.1	AP
4	2C-4C	1.394	1C-2C-4C	121.0	7C-1C-2C-19H	-1.0	–SP
5	2C-19H	1.085	1C-2C-19H	119.5	2C-1C-3C-5C	0.5	SP
6	3C-5C	1.393	4C-2C-19H	119.5	2C-1C-3C-20H	-178.1	–AP
7	3C-20H	1.083	1C-3C-5C	120.6	7C-1C-3C-5C	-179.2	–AP
8	4C-6C	1.393	1C-3C-20H	119.6	7C-1C-3C-20H	2.3	SP
9	4C-21H	1.085	5C-3C-20H	119.8	2C-1C-7C-8C	-117.0	–AC
10	5C-6C	1.395	2C-4C-6C	120.0	2C-1C-7C-14C	121.4	AC
11	5C-22H	1.085	2C-4C-21H	119.8	2C-1C-7C-24H	4.4	SP
12	6C-23H	1.084	6C-4C-21H	120.2	3C-1C-7C-8C	62.6	SC
13	7C-8C	1.557	3C-5C-6C	120.4	3C-1C-7C-14C	-59.0	–SC
14	7C-14C	1.526	3C-5C-22H	119.6	3C-1C-7C-24	-175.9	–AP
15	7C-24H	1.091	6C-5C-22H	120.0	1C-2C-4C-6C	0.2	SP
16	8C-9N	1.475	4C-6C-5C	119.5	1C-2C-4C-21	180.0	AP
17	8C-10C	1.544	4C-6C-23H	120.3	19H-2C-4C-6C	-179.7	–AP
18	8C-18H	1.093	5C-6C-23H	120.3	19H-2C-4C-21	0.1	SP
19	9N-11C	1.469	1C-7C-8C	113.7	1C-3C-5C-6C	-0.1	–SP
20	9N-25H	1.014	1C-7C-14C	110.6	1C-3C-5C-22H	-179.8	–AP
21	10C-12C	1.536	1C-7C-24H	107.8	20H-3C-5C-6C	178.5	AP
22	10C-26H	1.093	8C-7C-14C	107.9	20H-3C-5C-22H	-1.2	–SP
23	10C-27H	1.097	8C-7C-24H	109.4	2C-4C-6C-5C	0.2	SP
24	11C-13C	1.535	14C-7C-24H	107.2	2C-4C-6C-23H	179.9	AP
25	11C-28H	1.094	7C-8C-9N	108.6	21H-4C-6C-5C	-179.6	–AP
26	11C-29H	1.097	7C-8C-10C	113.5	21-4C-6C-23H	0.1	SP
27	12C-13C	1.534	7C-8C-18H	106.2	3C-5C-6C-4C	-0.3	–SP
28	12C-30H	1.097	9N-8C-10C	113.1	3C-5C-6C-23H	-180.0	–AP
29	12C-31H	1.094	9N-8C-18H	106.2	22H-5C-6C-4C	179.4	AP
30	13C-32H	1.098	10C-8C-18H	108.8	22H-5C-6C-23H	-0.3	–SP
31	13C-33H	1.096	8C-9N-11C	115.4	1C-7C-8C-9N	-177.0	–AP
32	14C-15O	1.207	8C-9N-25H	109.6	1C-7C-8C-10C	56.4	SC
33	14C-16O	1.349	11C-9N-25H	110.1	1C-7C-8C-18H	-63.1	–SC
34	16O-17C	1.440	8C-10C-12C	112.8	14C-7C-8C-9C	-53.9	–SC
35	17C-34H	1.088	8C-10C-26H	110.4	14C-7C-8C-10C	179.5	AP
36	17C-35H	1.091	8C-10C-27H	107.5	14C-7C-8C-18H	60.0	SC
37	17C-36H	1.091	12C-10C-26H	110.8	24H-7C-8C-9N	62.4	SC
38			12C-10C-27H	108.6	24H-7C-8C-10C	-64.2	–SC
39			26H-10C-27H	106.6	24H-7C-8C-18H	176.3	AP
40			9N-11C-13C	114.3	1C-7C-14C-15O	67.4	SC
41			9N-11C-28H	107.6	1C-7C-14C-16O	-111.2	–AC
42			9N-11C-29H	108.3	8C-7C-14C-15O	-57.6	–SC
43			13C-11C-28H	110.9	8C-7C-14C-16O	123.9	AC
44			13C-11C-29H	109.3	24H-7C-14C-15O	-175.3	–AP
45			28H-11C-29H	106.1	24H-7C-14C-16O	6.2	SP
46			10C-12C-13C	110.7	7C-8C-9N-11C	-80.4	–SC
47			10C-12C-30H	110.1	7C-8C-9N-25H	154.7	AP
48			10C-12C-31H	109.8	10C-8C-9N-11C	46.5	SC
49			13C-12C-30H	109.3	10C-8C-9N-25H	-78.4	–SC
50			13C-12C-31H	110.7	18H-8C-9N-11C	165.7	AP
51			30H-12C-31H	106.2	18H-8C-9N-25H	40.9	SC
52			11C-13C-12C	110.3	7C-8C-10C-12C	75.9	SC
53			11C-13C-32H	109.4	7C-8C-10C-26H	-48.5	–SC
54			11C-13C-33H	110.0	7C-8C-10C-27H	-164.4	–AP
55			12C-13C-32H	109.5	9C-8C-10C-12C	-48.4	–SC
56			12C-13C-33H	110.8	9C-8C-10C-26H	-172.8	–AP
57			32H-13C-33H	106.9	9C-8C-10C-27H	71.3	SC
58			7C-14C-15O	125.2	18-8C-10C-12C	-166.1	–AP
59			7C-14C-16O	111.4	18-8C-10C-26H	69.5	SC
60			15O-14C-16O	123.4	18-8C-10C-27H	-46.4	–SC
61			14C-16O-17C	115.8	8C-9N-11C-13C	-49.7	–SC

62		16O-17C-34H	105.5	8C-9N-11C-28H	-173.3	–AP
63		16O-17C-35H	110.3	8C-9N-11C-29H	72.4	SC
64		16O-17C-36H	110.5	25H-9N-11C-13C	74.9	SC
65		34H-17C-35H	110.7	25H-9N-11C-28H	-48.7	–SC
66		34H-17C-36H	110.7	25H-9N-11C-29H	-163.0	–AP
67		35H-17C-36H	109.3	8C-10C-12C-13C	52.9	SC
68				8C-10C-12C-30H	-68.1	–SC
69				8C-10C-12C-31H	175.4	AP
70				26H-10C-12C-13C	177.1	AP
71				26H-10C-12C-30H	56.1	SC
72				26H-10C-12C-31H	-60.4	–SC
73				27H-10C-12C-13C	-66.2	–SC
74				27H-10C-12C30H	172.8	AP
75				27H-10C-12C-31H	56.3	SC
76				9N-11C-13C-12C	52.9	SC
77				9N-11C-13C-32H	-67.5	–SC
78				9N-11C-13C-33H	175.4	AP
79				28H-11C-13C-12C	174.7	AP
80				28H-11C-13C-32H	54.3	SC
81				28H-11C-13C-33H	-62.8	–SC
82				29H-11C-13C-12C	-68.6	–SC
83				29H-11C-13C-32H	171.0	AP
84				29H-11C-13C-33H	53.9	SC
85				10C-12C-13C-11C	-54.1	–SC
86				10C-12C-13C-32H	66.3	SC
87				10C-12C-13C-33H	-176.1	–AP
88				30H-12C-13C-11C	67.4	SC
89				30H-12C-13C-32H	-172.2	–AP
90				30H-12C-13C-33H	-54.6	–SC
91				31H-12C-13C-11C	-176.0	–AP
92				31H-12C-13C-32H	-55.7	–SC
93				31H-12C-13C-33H	62.0	SC
94				7C-14C-16O-17C	-179.8	–AP
95				15O-14C-16O-17C	1.6	SP
96				14C-16O-17C-34H	-179.6	–AP
97				14C-16O-17C-35H	60.9	SC
98				14C-16O-17C-36H	-59.9	–SC

The shortest bond length is observed between 9N-25H (1.014 Å) while the largest bond distance is identified between 7C-8C (1.557 Å). From the dihedral angle values, it is clear that this molecule has synperiplanar (SP), synclinal (SC), antiperiplanar (AP) and anticlinal (AC) planar structures. Also, the dihedral angle data shows that the piperidine ring is in the chair conformation. The observed values matched with the earlier reports [19-21].

Mulliken charge: Table-3 displays the Mulliken charges computed at the B3LYP/6-311++G(d,p) level. Based on Table-3, a graph is generated and displayed in Fig. 2. It is observed that except for 1C, all other carbons have negative charges. 10C (-0.5051 a.u.) has the least charge and 1C (1.1565 a.u.) has the highest charge among carbon atoms. No negative charge is observed on the hydrogen atoms. The highest charge is on 24H and the lowest charge is on 30H. The charge on nitrogen is found to be -0.0699 a.u. 15O has the lowest charge (-0.1846 a.u.) and 16O has the highest value (0.0211 a.u.). Both are connected to the same carbon atom, whereas 16O is connected with a single bond.

TABLE-3
MULLIKEN CHARGE VALUES OF DEXMETHYLPHENIDATE

S. No.	Atom	Charge (a.u.)	S. No.	Atom	Charge (a.u.)	S. No.	Atom	Charge (a.u.)	S. No.	Atom	Charge (a.u.)
1	C	1.1565	10	C	-0.5051	19	H	0.1453	28	H	0.1849
2	C	-0.2327	11	C	-0.2210	20	H	0.1954	29	H	0.1300
3	C	-0.3758	12	C	-0.2562	21	H	0.1745	30	H	0.1177
4	C	-0.4052	13	C	-0.4594	22	H	0.1834	31	H	0.1833
5	C	-0.4772	14	C	-0.4871	23	H	0.1555	32	H	0.1269
6	C	-0.2998	15	O	-0.1846	24	H	0.3520	33	H	0.1617
7	C	-0.2294	16	O	0.0211	25	H	0.2634	34	H	0.1423
8	C	-0.1576	17	C	-0.2388	26	H	0.1509	35	H	0.1800
9	N	-0.0699	18	H	0.2282	27	H	0.1695	36	H	0.1773

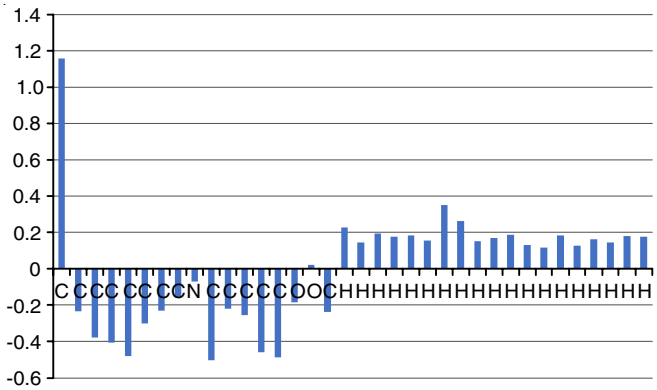

Fig. 2. Distribution of the Mulliken charge of dexmethylphenidate

Molecular electrostatic potential: The electrostatic potential values offer information about the shape, size, dipole moment, electronic density, interactions with hydrogen bonds, reactivity and other characteristics [22]. Red, blue, pale blue, green and yellow colours always represent the electrostatic potential of the molecule. The blue colour indicates the electron poor locations, while the red colour denotes the electron-rich domains.

The yellow colour signifies a location with a moderate abundance of electrons, while the pale blue colour denotes a region with a moderate deficiency of electrons. The presence of a neutral charge is generally shown by the green colour [23]. Fig. 3a highlights the 3D electrostatic potential map with varying colour representations. An intense red colour develops surrounding the oxygen atom, which is linked to carbon with a double bond and is highly vulnerable to electrophilic attack due to its rich electron density. It was observed that the molecule has green and light yellow colour representations in its various positions. The potential increases in the order of colour as red < orange < yellow < green < blue [24]. Additionally, the contour map was examined and it is evident from the map that the contour map penetrates through every atom (Fig. 3b). The energy range was calculated in the range from -5.076 e^{-2} to 5.076 e^{-2}.

Frontier molecular orbital: The frontier molecular orbital (FMO) energy gap helps to determine the chemical activity of molecule [25]. The chemical activities (molecular electrical transport, conductivity, kinetic stability and biological properties) can also be established from the FMO energy gap values [26]. Also, the molecular stability is enlightened by the difference between HOMO and LUMO [27]. A chemical and spectroscopic characteristics of the chemical structure are determined mainly by the energy gap [28]. The B3LYP/6-311++G(d,p) level of theory is utilized to calculate the HOMO and LUMO values. Table-4 shows the different physical parameters determined using the HOMO-LUMO values. The HOMO appears all over the piperidine ring and some regions of benzene ring. The LUMO has expanded over the phenyl ring, especially in some parts of the piperidine ring. 5.4423 eV is found to be the energy gap (Fig. 4). This wide gap implies the stability of the molecule. The HOMO and LUMO energies can be used to calculate the electron affinity (A), ionization potential (I) and other properties, which are shown in Table-4.

The HOMO and LUMO values of the molecule were used to determine directly the ionization potential (6.1498 eV) and the electron affinity (0.7075 eV) (Table-5), indicating that the molecule is hard and stable. The electron-donating capacity was found to be 4.2145 eV and the electron-accepting capacity was calculated as (0.7859 eV). These two values suggest that this molecule can act as an electron donor.

Non-covalent interaction: The software Multiwfn 3.8 was applied to survey the weak interaction of DMP. The non-covalent interaction was computed using the reduced density gradient (RDG) iso-surface function, which is defined as:

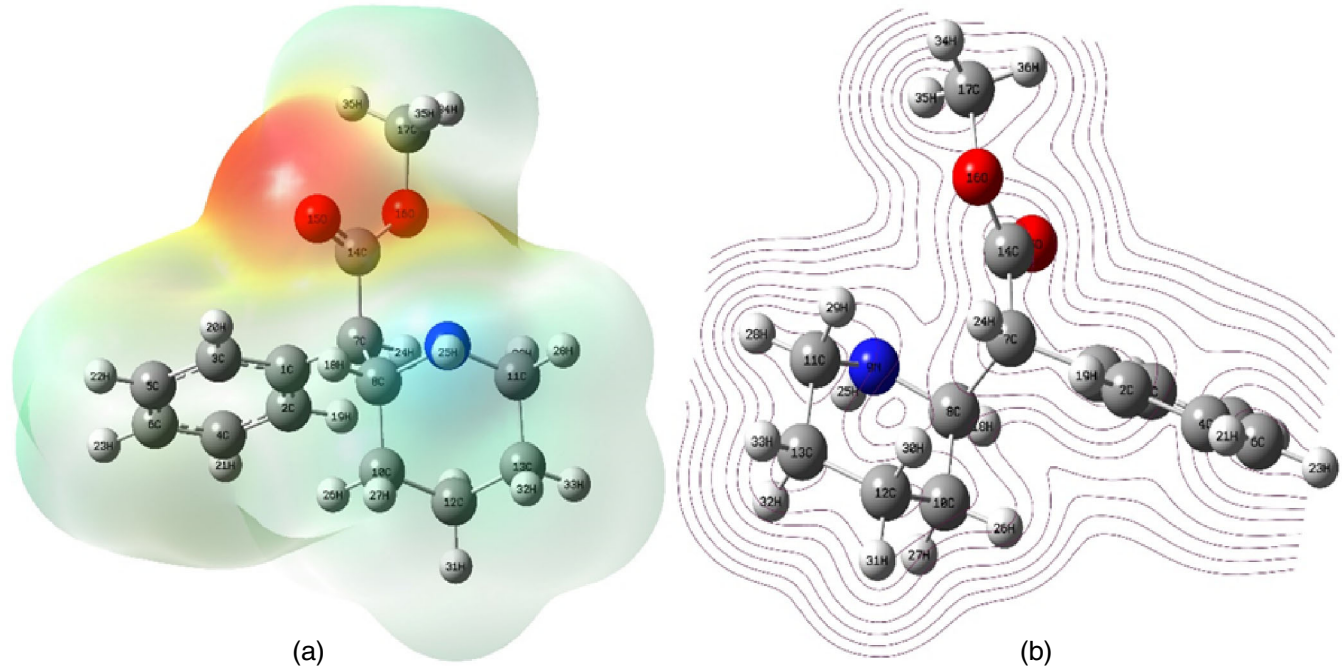

Fig. 3. (a) The electrostatic potential and (b) Contour diagram of dexmethylphenidate

TABLE-4
HOMO-LUMO AND DERIVED DATA FOR DEXMETHYLPHENIDATE

S. No.	Parameter	Formula	Charge (eV)	S. No.	Parameter	Formula	Charge (eV)
1	HOMO		-6.1498	10	Electrophilicity index (ω)	$\omega=\frac{\mu^2}{2\eta}$	2.16
2	LUMO		-0.7075	11	Electron accepting capability (ω^+)	$\omega^+=\frac{(I+3A)^2}{16(I-A)}$	0.7859
3	Energy gap (ΔE)		5.4423	12	Electron donating capability (ω^-)	$\omega^-=\frac{(3I+A)^2}{16(I-A)}$	4.2145
4	Ionization potential (I)	$I=-E_{HOMO}$	6.1498	13	Global softness (s)	$s=\frac{1}{2\eta}$	0.1837
5	Electron affinity (A)	$A=-E_{LUMO}$	0.7075	14	$\Delta E_{Back\ donation}$	$\Delta E=\frac{-\eta}{4}$	-0.6803
6	Electronegativity (χ)	$\chi=\frac{I+A}{2}$	3.4286	15	Nucleophilicity index (N)	$N=\frac{1}{\omega}$	0.463
7	Chemical potential (μ)	$\mu=-(\chi)$	-3.4286	16	Additional electronic charge (ΔN_{max})	$\Delta N_{max}=\frac{-\mu}{\eta}$	1.26
8	Chemical hardness (η)	$\eta=\frac{I-A}{2}$	2.7211	17	Optical softness (σ_0)	$\sigma_o=\frac{1}{\Delta E}$	0.1837
9	Chemical softness (S)	$S=\frac{1}{\eta}$	0.3675				

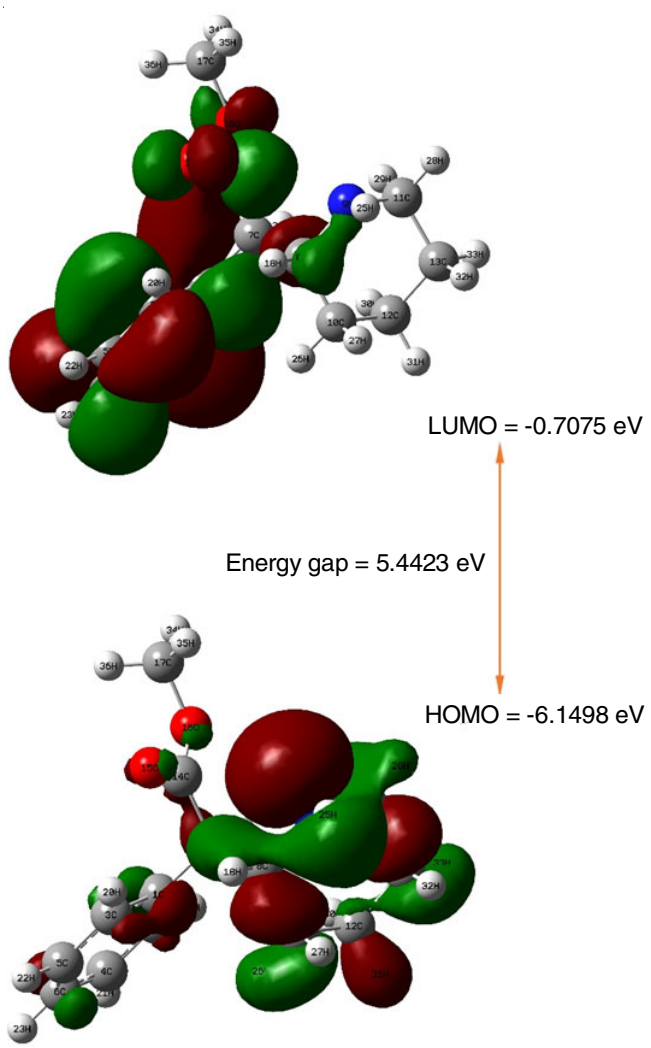

Fig. 4. The HOMO, LUMO and energy gap of dexmethylphenidate

$$RDG(r)=\frac{1}{2(3\pi)^{1/3}}\frac{|\nabla\rho(r)|}{\rho(r)^{4/3}} \quad (1)$$

The non-covalent interaction (NCI) is generated from the reduced density gradient (s) and the sign of λ_2 and multiplying the result by the density (ρ). A few spikes can be seen in the NCI plot's low-density area (Fig. 5), as it grows away from zero, the standard NCI interaction trace becomes stronger [29]. The iso-surface plot obtained by the VMD 1.9.4 tool was also presented alongside. The presence of a weak van der Waals attraction is responsible for the formation of spikes around the range of -0.010 to +0.010 a.u. The steric effect is indicated by the spikes nearer to +0.020 a.u. (Fig. 5a). The steric effect is represented by the red circle that can be seen between the piperidine and benzene rings in the iso-surface (Fig. 5b). The greenish-red iso-surfaces with low electron densities have been observed near the caves of the ester group, benzene ring and piperidine ring.

Hole-electron transfer: The software Multiwfn 3.8 is an unavoidable software for the analysis of electron excitation in a molecule. Additionally, it gives information about all types of electron transportation. It is a beneficial scheme for identifying the types of electron excitations [30]. The six lowest singlet excited states are examined at the same theoretical level. The Sm, Sr, H index, τ index, D index and excitation energy, Λ (Lambda) and Δr, along with the Coloumb attractive energies are investigated and tabulated in Table-5. Fig. 6 displays the hole-electron distribution, Sr function, c_{hole}–c_{elc} function and charge density difference (CDD).

The enormous D index value for S0→S5 excitation (2.303 Å) represents a charge transfer excitation (CT). For S0→S5 excitation (Fig. 6), there is a significant separation between the green (electron) and blue (hole) iso-surface centres. It is possible to express the D index for the excitations S0→S1, S2,

TABLE-5
THE HOLE-ELECTRON INTERACTION DETAILS FOR DEXMETHYLPHENIDATE

Excitation state	Sm (a.u)	Sr (a.u)	D (Å)	H (Å)	τ (Å)	Excitation energy (eV)	Coulomb energy (eV)	Δr (Å)	Λ
S1	0.795	0.959	0.062	2.109	-1.221	5.372	6.700	1.634	0.463
S2	0.132	0.331	1.747	2.442	0.443	5.489	4.913	1.978	0.233
S3	0.433	0.683	0.245	2.668	-0.960	5.806	5.375	1.938	0.377
S4	0.346	0.595	1.211	2.775	-0.759	5.951	5.045	2.390	0.320
S5	0.088	0.240	2.303	2.850	0.801	6.130	4.068	2.385	0.239
S6	0.452	0.658	1.515	2.958	-0.704	6.150	4.773	1.784	0.433

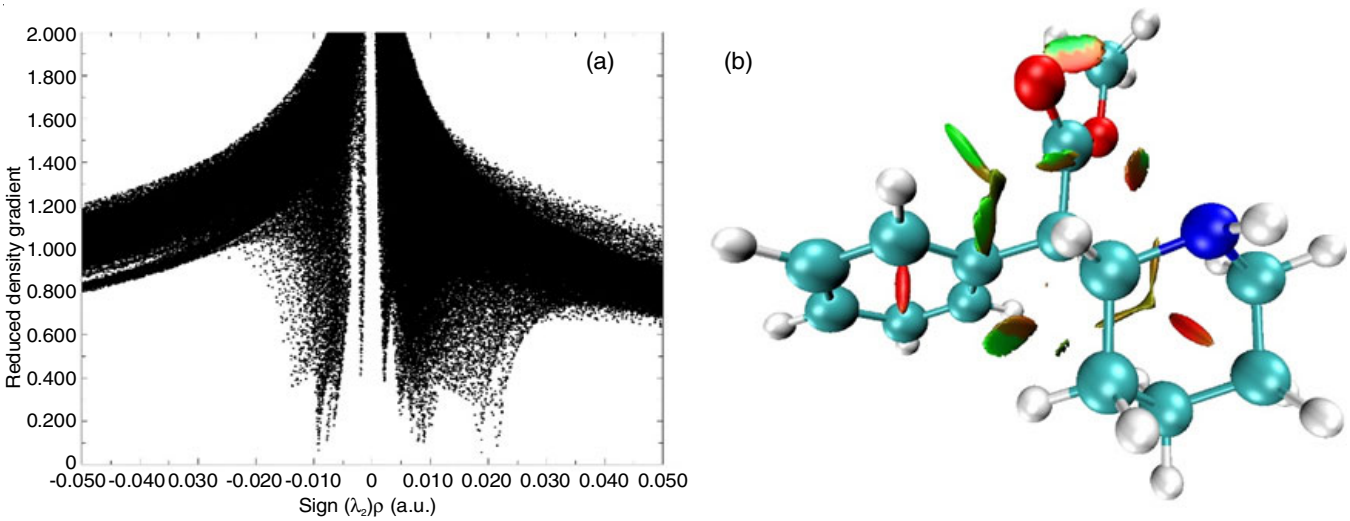

Fig. 5. (a) The NCI plot (b) iso-surface image for the headline molecule

S3, S4 and S6 as LE-type excitations since their values are not high.

The S0→S1 excitation state only has a higher Sr index (0.959 a.u.). All the other excited states have substantially scantier Sr index values (less than 0.8 a.u.). For a π→π* transition to occur, the Sr values must exceed 0.8 a.u. [31]. So S0→S2, S3, S4, S5 and S6 follow n→π* and S0→S1 transition follows a π→π* transition. The H index represents the dispersion of electrons and holes. The S0→S1 has a meagre H index value (2.109 Å). So, it is concluded that the electrons and holes are confined to a tiny region. The S0→S6 transition has a high H index value (2.958 Å), hence, it is thoroughly dispersed throughout the molecule (Fig. 6).

The positive τ index value of S0→S5 indicates a noticeable gap between the electrons and holes. Thus, it is understandable that the type of excitation is charge transfer (CT). For the other excitations from S0→S1, S2, S3, S4 and S6, the τ indices are remarkably negative, suggesting a very low degree of hole-electron separation and as a result, they are classified as the local excitation type (LE).

Table-5 demonstrates the correlation between the Coulomb attractive energy and the pair of electrons and holes in the parameters of electron excitation. The Coulomb energy decreases with an increasing D index and indicates a greater separation between the primary electron and hole distributions. It is clear from the results that the Coulomb attraction energy for S0→S5 (4.068 eV) is the lowest of all the excitations. Since the D index values of S0→S1, S2, S3, S4 and S6 are the modest, the excitation of these states results in a relatively confined spatial extent for these holes and electrons. Consequently, there is significant Coulomb attraction energy. S0→S1 has a meagre D index value (0.062 Å) and as a result, its Coulomb value is much bigger (6.700 eV).

The substantial Δr values (2.390 and 2.385 eV, respectively) of S0→S4 and S5 suggest that the excitation from these points may have a strong CT character. The Δr values are tiny for other excitations. The Δr value in the original publication proposes that 2.0 Å is required as a threshold to differentiate between CT and LE excitations [31]. S5 only follows charge transfer excitation, while the other excitations are local excitation (LE) type since it has positive τ and large Δr values.

There is almost an inverse relationship between the Δr values and the lambda (Λ) values. The hole-electron separation distance is typically shorter the higher the hole-electron overlapping area. The shortest Δr (1.634 Å) value is seen in the S0→S1 excited state among all excitations and the correlated lambda value is estimated at 0.463. The following findings are drawn from Table-5 and the aforementioned iso-surface maps (Fig. 5):

S0→S1 local excitation (π→π*)
S0→S2 local excitation (n→π*)
S0→S3 local excitation (n→π*)
S0→S4 local excitation (n→π*)
S0→S5 charge transfer excitation (n→π*)
S0→S6 local excitation (n→π*)

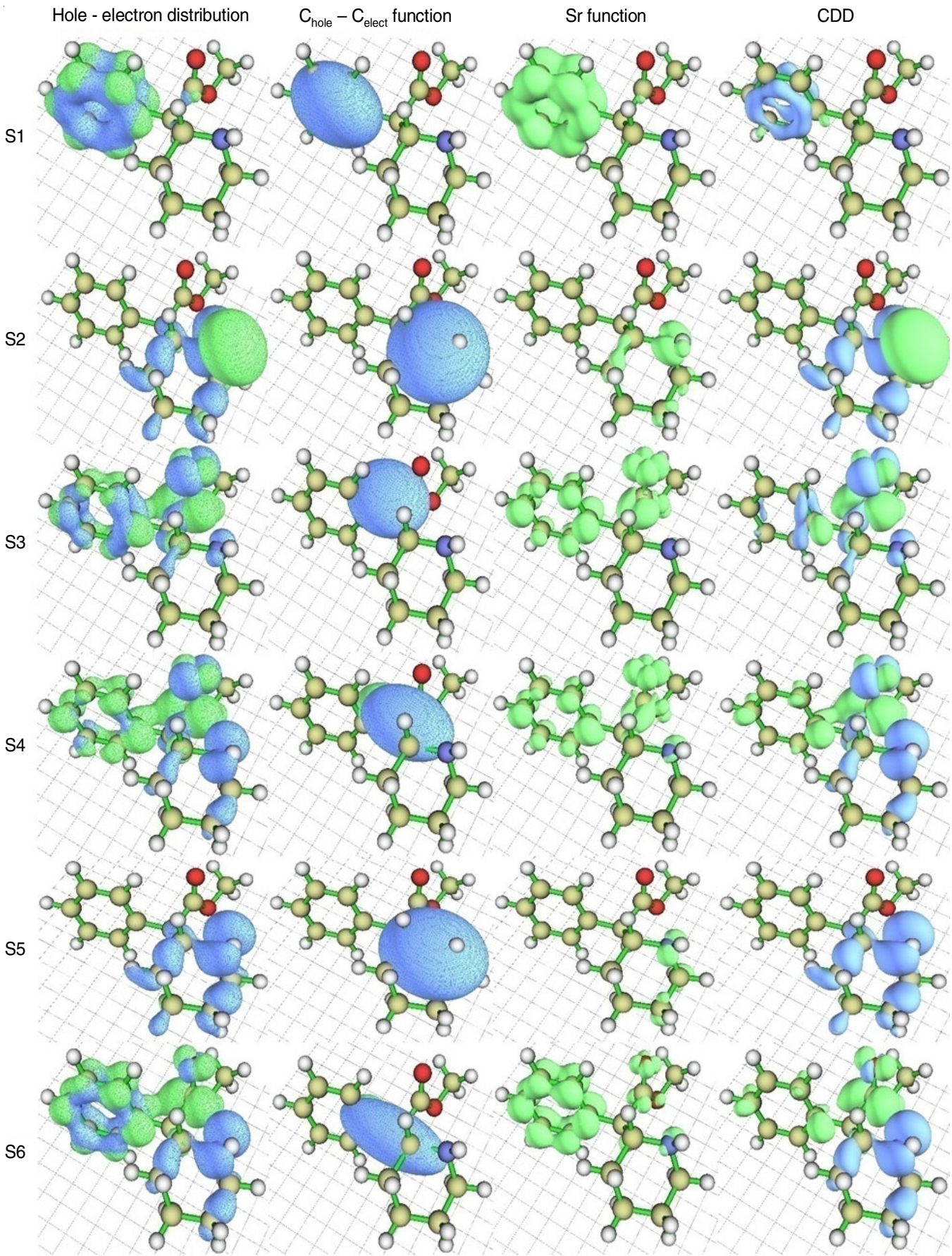

Fig. 6. The title molecule's hole-electron distribution (HED), c_{hole} – c_{elec} function, Sr and charge density difference for the first six excitations

Heat map: Based on the findings of hole-electron analysis, a heat map can be used to investigate the buildup of electrons and holes. It was used quantitatively to investigate the amount of charge transfer between different fragments for the lowest six excitation states. For this type of scheming, the optimized molecule with the B3LYP/6-311++G(d,p) basis set is subjected to analysis with the TDDFT/CAM-B3LYP basis set. The IO*p* (9/40=4) keyword is used (n=6 state conditions). The fragmentation pattern of the title molecule is shown in Fig. 7.

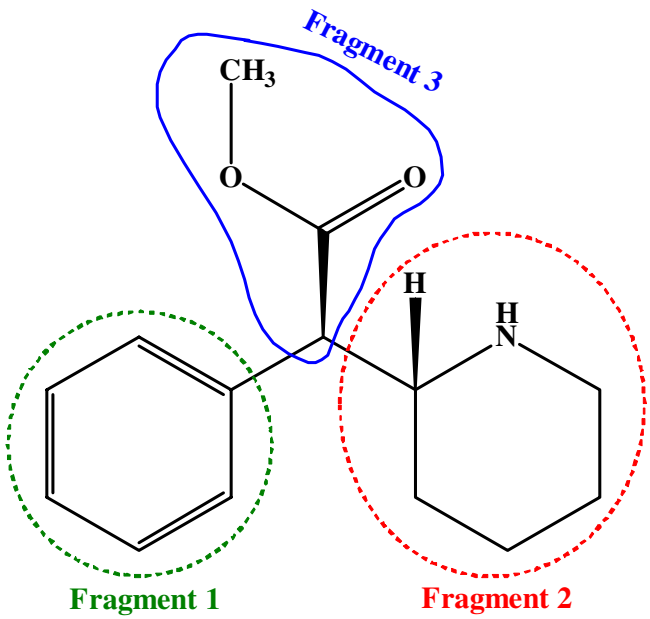

Fig. 7. Fragmentation pattern of DMP used to create heat maps

The heat maps are generated to visualize the natural phenomena in the six lowest excitation states. The calculated percentages of hole, electron, overlap and difference are shown in Table-6 and the generated heat maps for the lowest six excitations are illustrated in Fig. 8.

From Table-6 and Fig. 8, the observations were made *viz*. In the S0 → S1 excitation, the amount of electrons is rich in the benzene ring. In S0→S2 excitation, the electrons are rich in fragment 2 (piperidine). The side chain has more holes in the S0→S3 excitation. Benzene has more electrons in S0→S4 and S6, while fragment 2 has more electrons in S0→S5.

Aromaticity: The molecule under investigation has an aromatic benzene ring in its structure. Its aromaticity is compared with benzene and toluene at the same level of theory. The para delocalization index (PDI) [32], aromatic fluctuation index (FLU) [33], harmonic oscillator measure of aromaticity (HOMA) [34] and bird aromaticity [35] values were obtained from the Multiwfn 3.8 tool and tabulated in Table-7. The FLU (eqn. 2), PDI (eqn. 3), HOMA (eqn. 4) and bird aromaticity (eqn. 5) are defined as:

$$FLU = \frac{1}{n}\sum_{A-B}^{ring}\left[\left(\frac{V(B)}{V(A)}\right)^{\alpha}\left(\frac{\delta(A,B)-\delta_{ref}(A,B)}{\delta_{ref}(A,B)}\right)\right]^2 \quad (2)$$

where n is equal to the number of atoms in ring; δ_{ref} is the reference DI value, which is the pre-calculated parameter; α is used to ensure the ratio of atomic valences is greater than one.

$$PDI = \frac{\delta(1,4)+\delta(2,5)+\delta(3,6)}{3} \quad (3)$$

$$HOMA = 1-\sum_{i}\frac{\alpha_{i,j}}{N}(R_{ref}-R_{i,j})^2 \quad (4)$$

where N is the total number of the atoms considered; α and R_{Ref} are pre-calculated constants; j means the atom next to atom i.

$$I = 100\left[1-\left(\frac{V}{V_K}\right)\right] \quad \text{where}$$

$$V = \frac{100}{\overline{N}}\sqrt{\frac{\sum_{i}(N_{i,j}-\overline{N})^2}{n}} \qquad N_{i,j} = \frac{a}{R_{i,j}}-b \quad (5)$$

TABLE-6
THE PERCENTAGE OF HOLES, ELECTRONS, OVERLAP AND DIFFERENCE UNDER THE HEAT MAP GENERATION STUDY FOR DEXMETHYLPHENIDATE

Excitation	Fragment	Hole (%)	Electron (%)	Overlap (%)	Difference (%)
S1	1. Benzene	112.94	121.10	116.95	8.16
	2. Piperidine	17.83	19.96	18.87	2.14
	3. Side chain	17.77	17.56	17.66	-0.21
S2	1. Benzene	3.59	-29.76	0.00	-33.35
	2. Piperidine	99.68	113.78	106.49	14.10
	3. Side chain	-1.54	-0.76	0.00	0.79
S3	1. Benzene	45.18	54.87	49.79	9.69
	2. Piperidine	12.68	25.95	18.14	13.27
	3. Side chain	61.93	51.30	56.36	-10.63
S4	1. Benzene	29.02	60.43	41.88	31.41
	2. Piperidine	44.57	21.95	31.28	-22.61
	3. Side chain	39.03	50.03	44.19	11.00
S5	1. Benzene	7.13	-27.71	0.00	-34.85
	2. Piperidine	96.85	119.62	107.63	22.77
	3. Side chain	-0.74	-23.88	0.00	-23.14
S6	1. Benzene	49.58	71.29	59.45	21.71
	2. Piperidine	59.03	31.86	43.37	-27.17
	3. Side chain	12.49	37.51	21.64	25.02

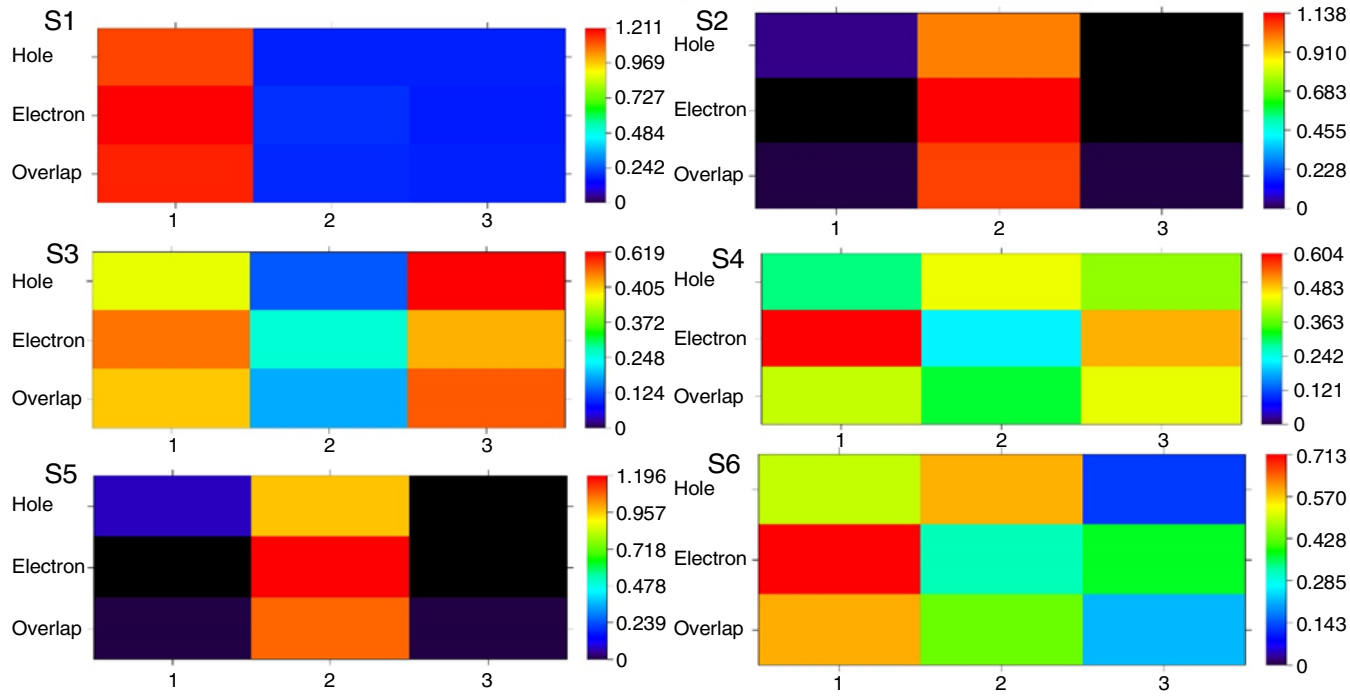

Fig. 8. Heat maps generated for the lowest six excitations for the dexmethylphenidate (the colour scale for all six excitations is not on the same scale)

TABLE-7
PDI, FLU, HOMA AND BIRD AROMATICITIES FOR DEXMETHYLPHENIDATE, BENZENE AND TOLUENE

Molecule	PDI	FLU	HOMA	Bird
Benzene	0.1045	0.000021	0.9888	99.9064
Toluene	0.1012	0.000738	0.9835	97.8780
Dexmethylphenidate	0.1002	0.001116	0.9824	97.4741

where 'i' cycles all of the bonds in the ring; j signifies the atom next to atom i; n is the total number of the bonds considered. The N/N symbolizes Gordy bond order, is the average value of the N values; $R_{i,j}$ is bond length, a and b are predefined parameters, respectively, for each type of bond; V_K is a pre-determined reference V.

Table-7 shows that the PDI value is almost the same for DMP, benzene and toluene. It is known that if the value of FLU is small, it will show a high aromatic nature. In DMP, the aromaticity is slightly less than that of the other two molecules. When HOMA is 1, every bond's length corresponds to the ideal value of R_{Ref}, indicating that the ring is entirely aromatic. From Table-7, it is clear that the aromaticity of benzene is higher than that of the studied molecule. If the Bird value is closer to 100, it has more aromaticity. Table-7 shows that the test molecule is slightly less aromatic than benzene.

Scanning tunnelling microscope: A conducting probe and sharp metallic tips capture the spatial fluctuations in the tunnelling current. This opinion is utilized in the scanning tunnelling microscope [36]. The Multiwfn 3.8 tool has been used to generate and analyze the simulated scanning tunnelling microscope image for the title molecule. At V = -3.5 and Z = 2.2 Å, the investigated molecule's local density of states (LDOS) value is determined to be 0.0381 a.u. (Fig. 9). The larger the LDOS and consequently, the stronger the tunnelling current

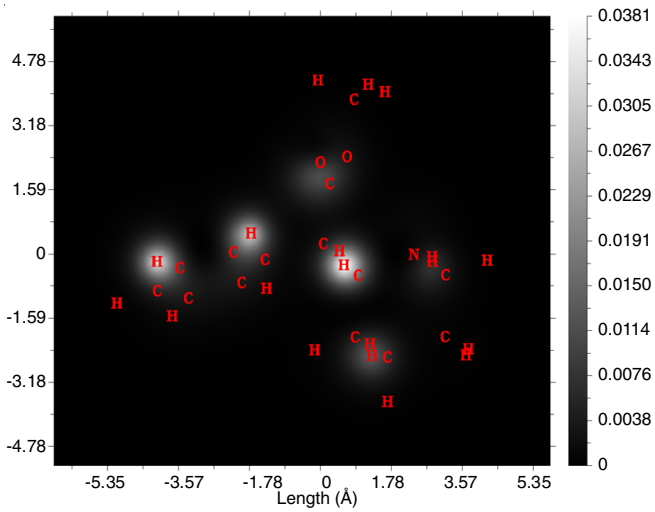

Fig. 9. STM image of dexmethylphenidate molecule

(I) on this map, the brighter the white. According to the Tersoff-Hamann model, 'I' has a positive relationship with LDOS. It can be seen that the 'I' signal is more prominent almost over the molecule, except for the CH_3 group.

Shaded surface map (with a projection) of localized orbital locator (LOL) determination: A shaded surface map with a projection of LOL (eqn. 6) is a function for locating high localization regions. It is generally defined by Schmider and Becke [37,38].

$$LOL(r) = \frac{\tau(r)}{1+\tau(r)} \quad (6)$$

where '$\tau(r)$ (dimensionless variable) is $g_0(r)/g_{(r)}$'. In general positive one electron kinetic energy is required and is defined as:

$$g(r) = \frac{1}{2}\sum \nabla_{\psi_i}(r)\nabla\psi_i(r) \quad (7)$$

where 'Ψ_i (r) is the Hatree-Fock or the Kohn-Sham orbital'.

The likelihood that electron motion is restricted within a region increases with the size of LOL in that region. Fig. 10 displays the shaded surface map of the title molecule, including a projection, after undergoing theoretical assessment using the localized orbital locator (LOL). Fig. 10a-b displays a perspective of the piperidine and aromatic benzene rings. The colour red symbolizes the elevated electron density of the nitrogen atom, whereas all carbon atoms are blue, indicating depleted electron regions. The high-localized electron regions are present in aromatic hydrogen atoms and there is electron depletion in the central area of the carbon atoms. The oxygen atoms of the ester and methyl groups are abundant in electrons (Fig. 10c). The electrons tend to concentrate on their outer edges to stabilize the rings.

Simulated UV-visible studies: At the B3LYP/6-311++ G(d,p) level of theory, the TD-DFT calculations have been performed to predict the electronic transitions, their contributions (major and minor), the excitation energies, absorption spectrum, absorption wavelengths and oscillator strengths for the title molecule. This work is performed in various solvents like DMSO, benzene, carbon tetrachloride, water, ethanol, acetone, methanol and THF. The results obtained by the ethanol solvent were used for the delineation. The polarizable continuum model using the integral equation formalism variant (IEFPCM) solvation model is considered for the calculation. Table-8 listed the major and minor contributions of the transitions along with

TABLE-8
SIMULATED UV-VIS DATA OBTAINED FOR DEXMETHYLPHENIDATE IN VARIOUS SOLVENTS

Solvent	Energy (cm^{-1})	Calculated wavelength (nm)	Osc. strength (f)	Major contributions	Minor contributions
Ethanol	37815.30	264.4	0.0057	HOMO→LUMO (96%)	HOMO→LUMO+6 (3%)
	40572.11	246.5	0.0009	HOMO→LUMO+1 (90%)	HOMO-2→LUMO (6%), HOMO-1→LUMO+1 (3%)
	42052.94	237.8	0.0154	HOMO→LUMO+2 (74%) HOMO→LUMO+3 (22%)	–
Benzene	38301.65	261.1	0.0082	HOMO→LUMO (96%)	HOMO→LUMO+6 (3%)
	40710.83	245.6	0.001	HOMO→LUMO+1 (87%)	HOMO-2→LUMO (7%), HOMO-1→LUMO+1 (4%)
	41314.94	242.0	0.0158	HOMO→ LUMO+2 (72%), HOMO→LUMO+3 (22%)	–
CCl_4	38310.53	261.0	0.008	HOMO→LUMO (96%)	HOMO→LUMO+6 (3%)
	40715.67	245.6	0.001	HOMO→LUMO+1 (87%)	HOMO-2→LUMO (7%), HOMO-1→LUMO+1 (4%)
	41308.49	242.1	0.0155	HOMO→LUMO+2 (72%), HOMO→LUMO+3 (22%)	–
Water	37774.17	264.7	0.0055	HOMO→LUMO (96%)	HOMO→LUMO+6 (2%)
	40568.88	246.5	0.0009	HOMO→LUMO+1 (90%)	HOMO-2→LUMO (6%), HOMO-1→LUMO+1 (3%)
	42119.89	237.4	0.0152	HOMO→LUMO+2 (74%) HOMO→LUMO+3 (21%)	–
Acetone	37829.06	264.3	0.0057	HOMO→LUMO (96%)	HOMO→LUMO+6 (3%)
	40573.72	246.5	0.0009	HOMO→LUMO+1 (90%)	HOMO-2→LUMO (6%), HOMO-1→LUMO+1 (3%)
	42034.39	237.9	0.0153	HOMO→LUMO+2 (74%) HOMO→LUMO+3 (21%)	HOMO→LUMO+3 (22%)
Methanol	37815.30	264.4	0.0057	HOMO→LUMO (96%)	HOMO→LUMO+6 (3%)
	40572.10	246.5	0.0009	HOMO→LUMO+1 (90%)	HOMO-2→LUMO (6%), HOMO-1→LUMO+1 (3%)
	42052.94	237.8	0.0154	HOMO→LUMO+2 (74%) HOMO→LUMO+3 (22%)	–
THF	37950.81	263.5	0.0063	HOMO→LUMO (96%)	HOMO→LUMO+6 (3%)
	40595.50	246.3	0.0009	HOMO→LUMO+1 (90%)	HOMO-2→LUMO (6%), HOMO-1→LUMO+1 (3%)
	41844.04	239.0	0.0156	HOMO→LUMO+2 (73%) HOMO→LUMO+3 (23%)	–
DMSO	37785.46	264.7	0.0058	HOMO→LUMO (96%)	HOMO→LUMO+6 (3%)
	40568.07	246.5	0.0009	HOMO→LUMO+1 (90%)	HOMO-2→LUMO (6%), HOMO-1→LUMO+1 (3%)
	42088.43	237.6	0.0157	HOMO→LUMO+2 (74%), HOMO→LUMO+3 (21%)	–

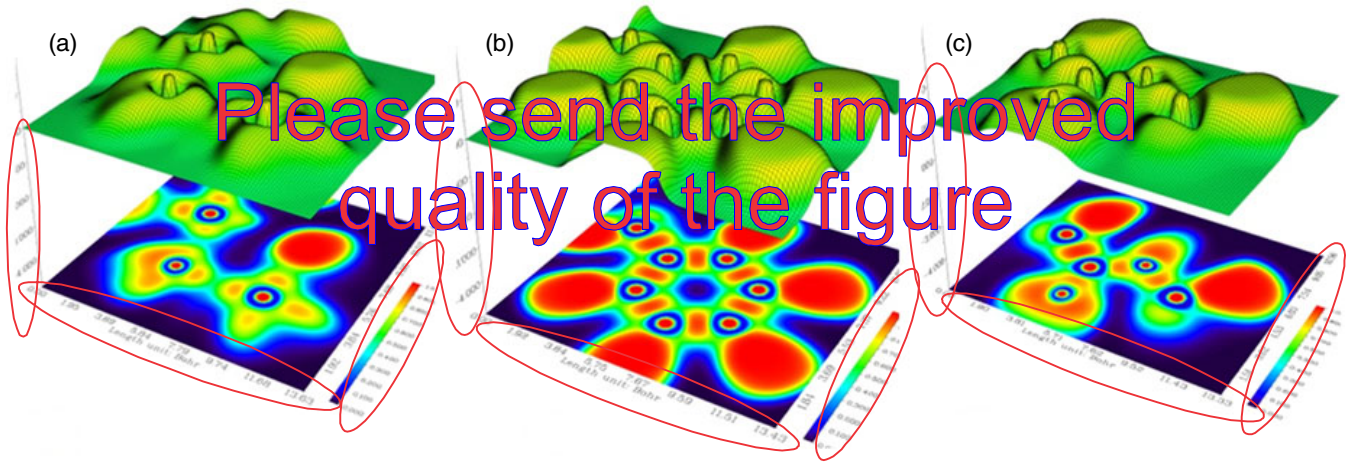

Fig. 10. Shaded surface map (with a projection effect of electron localization function) of the title molecule. (Here, the Z-axis denotes the localized orbital locator (LOL))

absorption wavelengths (λ), oscillator strengths (f) and excitation energies (E) for various solvents.

Fig. 11 shows the simulated UV-Vis spectra of DMP in various solvents. It is anticipated that there are three strong electronic transitions at 264.4, 246.5 and 237.8 nm, respectively, for ethanol solvent. At 237.8 nm, the oscillator strength (0.0154) is at its highest and the HOMO evolves at the 65th orbital.

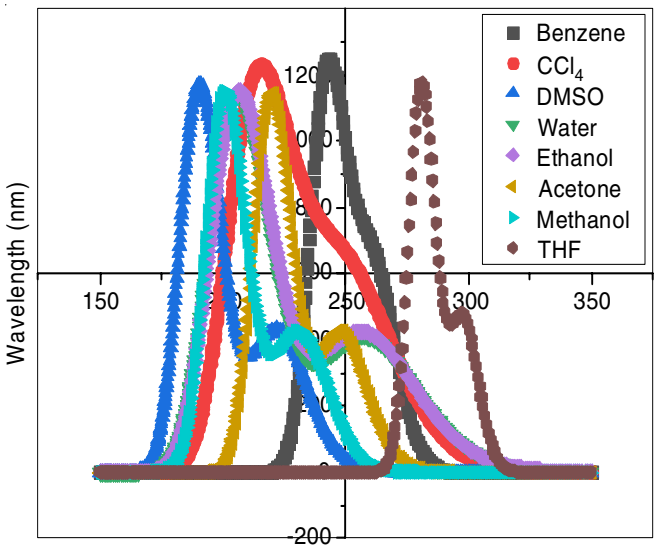

Fig. 11. Simulated UV-Vis plot generated for dexmethylphenidate in various solvents

With an energy of 37815.30 cm^{-1}, the signal at 264.4 nm is produced by the major electronic excitation of HOMO→LUMO (96%) and the minor contribution of HOMO→LUMO +6 (3%). The peak at 246.5 with an energy of 40572.11 cm^{-1} is due to the major contributions of HOMO→LUMO+1 (90%) and the minor contribution of HOMO-2→ LUMO (6%) as well as HOMO-1→LUMO+1 (3%). The major contributions of HOMO→LUMO+2 (74%) and HOMO→LUMO+3 (22%) are the reasons for the development of a peak at 237.8 nm with an energy of 42052.94 cm^{-1}.

Fukui function: The Fukui functions (FF) can be used to gain insight into reactivity indices. This function, sometimes known as electrophilic or nucleophilic attack sites, is based on the presumptions of which atoms in a molecule can acquire or lose an electron [39]. The partial derivative of the electron density ρ(r) is the total number of electrons (N); in the system with a constant external potential ν(r). The definition of the Fukui function is as follows:

$$f(r) = \left(\frac{\delta\rho(r)}{\delta(N)}\right)_{\nu(r)} \quad (8)$$

when a molecule takes on an electron, its Fukui function is f_k^+ (nucleophilic attack index). Similarly, the Fukui functions or f_k^- (index of electrophilic attack), if a molecule has a propensity to lose an electron [40]. On the other hand, condensed Fukui functions are used to quantify the Fukui function, *i.e.* to give a numerical value to each atom in a molecular system that represents its possibility of acting as a reactive site. The following condensed Fukui functions represent the electrophilic, nucleophilic and radical attacks:

$$f^+(r) = qk(N+1) - qk(N) \quad (9)$$

$$f^-(r) = qk(N) - qk(N-1) \quad (10)$$

$$f^0(r) = \left[\frac{qk(N+1) - qk(N-1)}{2}\right] \quad (11)$$

where qk is the electronic population of atom k in neutral (N), (N-1) cationic and (N+1) anionic states. Morrel *et al.* [41] proposed the descriptor Δf(r) for nucleophilicity and electrophilicity, which is defined as follows:

$$\Delta f(r) = [f_k^+ - f_k^-] \quad (12)$$

If Δf(r) > 0, then the site is electrophilic and if Δ (f) < 0, then the site is nucleophilic attacks. This theory describes the dual descriptor that can identify the type of reactive sites.

The Mulliken population analysis (MPA) and natural population analysis (NPA) were determined for the title molecule under the same basis set. The Fukui functions (f_k^+), (f_k^-), ($f^0(r)$) and Δf(r) values are listed in Table-9 and based on these values, three plots are generated as shown in Fig. 12.

TABLE-9
THE CONDENSED FUKUI FUNCTIONS (f_k^+), (f_k^-), ($f^0(r)$) AND DUEL DESCRIPTOR $\Delta f(r)$ FOR DEXMETHYLPHENIDATE

S. No.	Atom	Natural population analysis (NPA)				Mulliken population analysis (MPA)		
		f_k^-	$f^0(r)$	f_k^+	$\Delta f(r)$	f_k^-	$f^0(r)$	f_k^+
1	1C	0.6486	0.7761	0.7883	0.1397	-0.2720	1.1565	0.1389
2	2C	-0.2255	-0.3485	-0.2999	-0.0744	1.4181	-0.2327	0.0032
3	3C	-0.3697	-0.3848	-0.3446	0.0251	-0.2825	-0.3758	0.0369
4	4C	-0.1121	-0.1037	-0.1131	-0.0010	-0.3315	-0.4052	-0.0073
5	5C	-0.0548	-0.0788	-0.0883	-0.0335	0.1335	-0.4772	-0.0115
6	6C	-0.0048	-0.1827	-0.0317	-0.0269	-0.9892	-0.2998	0.1718
7	7C	-1.8669	-1.5872	-1.5245	0.3424	-1.1454	-0.2294	0.0458
8	8C	1.1974	0.5769	0.2754	-0.9220	-0.2016	-0.1576	-0.0209
9	9N	-0.7339	-0.7162	-0.2796	0.4543	0.1520	-0.0699	0.4815
10	10C	0.4243	-0.2718	-0.1749	-0.5992	-0.2018	-0.5051	0.0733
11	11C	0.9267	0.2336	0.0742	-0.8525	-0.3064	-0.2210	-0.0103
12	12C	1.0386	0.2232	0.0626	-0.9760	0.0097	-0.2562	0.0004
13	13C	0.8704	-0.1979	-0.1638	-1.0342	-1.2273	-0.4594	0.0589
14	14C	1.3277	1.0774	1.1077	-0.2200	-0.0333	-0.4870	0.0025
15	15O	-0.6871	-0.5746	-0.5453	0.1418	0.0176	-0.1846	0.0208
16	16O	-0.4882	-0.3366	-0.3459	0.1423	0.0285	0.0211	0.0000
17	17C	0.7408	-0.0927	-0.1277	-0.8685	-0.5273	-0.2388	0.0017
18	18H	-0.2118	0.0417	0.1160	0.3278	0.1995	0.2282	-0.0010
19	19H	0.0875	0.1725	0.1889	0.1014	0.3981	0.1453	-0.0038
20	20H	0.1920	0.2136	0.2280	0.0360	0.0365	0.1954	-0.0028
21	21H	-0.0412	0.1293	0.1616	0.2028	0.5751	0.1745	-0.0002
22	22H	-0.0030	0.1235	0.1562	0.1592	0.3025	0.1834	-0.0003
23	23H	-0.0652	0.1347	0.1470	0.2122	0.4155	0.1555	-0.0085
24	24H	0.4137	0.4061	0.4045	-0.0092	-0.1666	0.3520	0.0037
25	25H	-0.0034	0.3100	0.3183	0.3217	0.1778	0.2634	-0.0065
26	26H	-0.2025	0.0780	0.1105	0.3130	-0.1984	0.1509	0.0042
27	27H	-0.4423	0.0423	0.0866	0.5289	0.5188	0.1695	-0.0005
28	28H	-0.3817	0.0196	0.0815	0.4632	0.6203	0.1849	0.0026
29	29H	-0.3539	0.0220	0.0995	0.4534	0.0553	0.1300	0.0121
30	30H	-0.4404	-0.0194	0.0355	0.4759	0.0431	0.1177	0.0003
31	31H	-0.5197	-0.0260	0.0621	0.5818	0.5605	0.1833	0.0134
32	32H	-0.4832	0.0518	0.0834	0.5666	0.1276	0.1269	-0.0014
33	33H	-0.5254	0.0201	0.0945	0.6199	0.4878	0.1617	0.0026
34	34H	-0.2547	0.1034	0.1389	0.3936	0.2974	0.1423	0.0001
35	35H	-0.1943	0.0851	0.1052	0.2995	0.1347	0.1800	0.0001
36	36H	-0.2019	0.0799	0.1129	0.3148	0.1732	0.1773	-0.0001

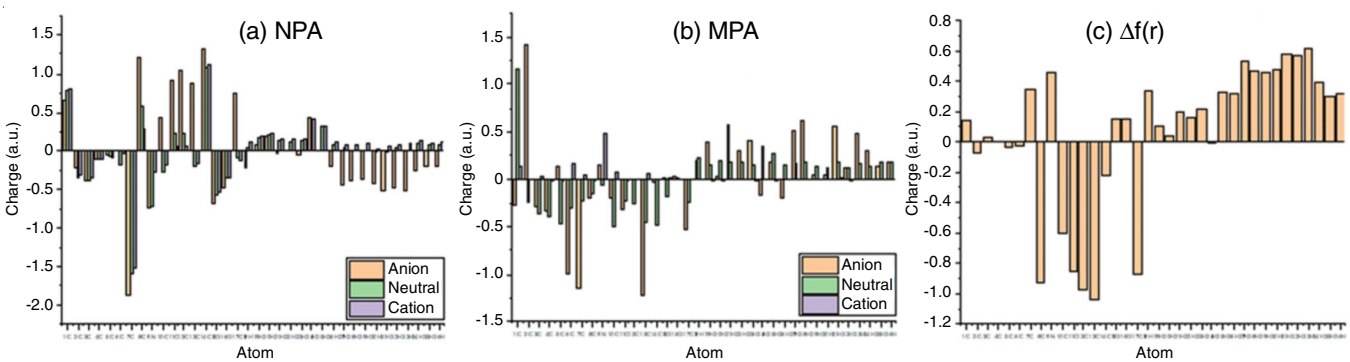

Fig. 12. (a) Natural population analysis (NPA), (b) Mulliken population analysis (MPA) and (c) Δf(r) values obtained for dexmethylphenidate

According to natural population analysis (NPA) calculations for neutral, anionic and cationic species, the electrophilic attack is possible at 7C in common and the nucleophilic attack is common at 14C for the three types of radicals. Since the value at 7C is higher than 14C for these species, the electrophilic attack is easy. For anionic species, the electrophilic attack is possible in the order of 7C > 9N > 15O > 33H > 31H > 16O and so on, while the nucleophilic attack is possible in the order of 14C > 8C > 12C > 11C > 13C > 17C and so on. In case of neutral radicals, the electrophilic attack is in the order of 7C > 9N > 15O > 3C > 2C > 16O and so on. The nucleophilic attack is found to follow the order of 14C > 1C > 8C > 24H > 25H > 11C and so on. For the cationic species, the electrophilic and nucleophilic attacks are in the orders of 7C > 15O > 16O > 3C

> 2C > 9N and 14C > 1C > 24H > 25H > 8C > 20H, respectively. According to MPA calculations, the chances of electrophilic attack for anionic, neutral and cationic radicals are in the following order: 13C > 7C > 6C > 17C > 4C > 11C; 10C > 14C > 5C > 13C > 4C > 3C; and 8C > 5C > 11C > 23H > 4C > 25H, respectively. Similarly, the nucleophilic attacks for radicals mentioned above are found to be: 2C > 28H > 21H > 31H > 27H > 33H; 1C > 24H > 25H > 18H > 20H > 28H; and 9N > 6C > 1C > 10C > 13C > 7C, respectively. The molecule as a whole is more vulnerable to nucleophilic attack at various atoms, according to the Δf(r) results. The atoms with almost zero values in NPA and MPA calculations are possible sites for free radical attack.

Simulated vibrational frequency: Quantifying the interactivity between infrared radiation (IR) and a molecule yields vibrational spectroscopic data. This molecule vibrates in 102 group modes (vibrational and fingerprint vibrations) with 36 atoms distributed across different planes. Out of the 102 usual vibration modes, 45 are out-of-plane and 57 are in-plane. A′ represents the molecule's in-plane bands and A″ represents its out-of-plane bands. Thus, Γ_{Vib} = 57 A′ + 45 A″ represents the distribution of the title molecule's 102 normal modes of vibration. The theoretical vibrations for the title molecule are computed using the DFT/B3LYP/6-311++G(d,p) basis set and are tabulated in Table-10. The resulting infrared spectrum is displayed in Fig. 13. By employing the 6-311G basis set, the theoretical values are compared with the calculated values, revealing a significant level of agreement. The scaling factors used were 0.9663 (6-311) and 0.9668 (6-311++G(d,p).

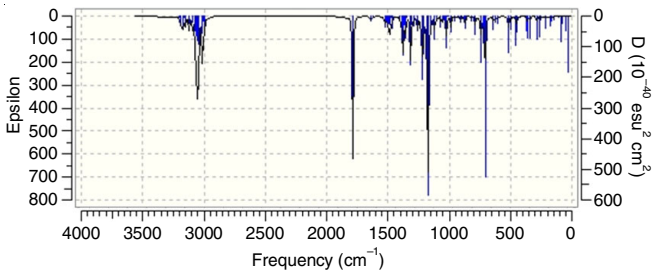

Fig. 13. Simulated IR spectrum of the target molecule at the DFT/B3LYP/6-311++G(d,p) level of theory

TABLE-10
SIMULATED VIBRATIONAL FREQUENCY ANALYSIS OF THE TITLE MOLECULE UNDER THE 6-311G AND 6-311++G(d,p) BASIS SET WITH PED FOR DEXMETHYLPHENIDATE

S. No.	S^y	Frequency				Intensity	Assignments with PED (%)
		6-311G	Scaled value	6-311++G(d,p)	Scaled value		
1	A′	3545	3425	3533	3415	vw	τ $^{9}N^{25}H$ (100)
2	A′	3203	3095	3195	3089	vw	τ $^{3}C^{20}H$ (79), τ $^{5}C^{22}H$ (15)
3	A′	3191	3083	3186	3080	vw	τ $^{3}C^{20}H$ (12), τ $^{4}C^{21}H$ (33), τ $^{6}C^{23}H$ (43)
4	A′	3176	3069	3174	3069	w	τ $^{2}C^{19}H$ (17), τ $^{4}C^{21}H$ (34), τ $^{5}C^{22}H$ (33), τ $^{6}C^{23}H$ (11)
5	A′	3172	3065	3164	3059	vw	τ $^{2}C^{19}H$ (27), τ $^{5}C^{22}H$ (40), τ $^{6}C^{23}H$ (29)
6	A′	3164	3057	3156	3052	vw	τ $^{2}C^{19}H$ (50), τ $^{4}C^{21}H$ (30), τ $^{6}C^{23}H$ (13)
7	A′	3155	3049	3154	3049	vw	ϕ $^{17}C^{34}H$ (80), γ $^{17}C^{35}H$ (10), γ $^{17}C^{36}H$ (10)
8	A′	3132	3026	3123	3020	vw	ϕ $^{17}C^{35}H$ (50), ϕ $^{17}C^{36}H$ (50)
9	A′	3096	2992	3094	2991	vw	τ $^{7}C^{24}H$ (93)
10	A′	3066	2963	3070	2968	w	ϕ $^{10}C^{26}H$ (70), ϕ $^{10}C^{27}H$ (30)
11	A′	3064	2961	3065	2963	m	τ $^{11}C^{28}H$ (80), ϕ $^{11}C^{29}H$ (14)
12	A′	3056	2953	3062	2961	vw	τ $^{8}C^{18}H$ (91)
13	A′	3050	2947	3053	2952	m	ϕ $^{12}C^{30}H$ (19), ϕ $^{12}C^{31}H$ (64)
14	A′	3047	2944	3050	2949	w	γ $^{17}C^{34}H$ (20), γ $^{17}C^{35}H$ (40), γ $^{17}C^{36}H$ (40)
15	A′	3041	2938	3046	2945	m	τ $^{12}C^{31}H$ (14), ϕ $^{13}C^{32}H$ (13), ϕ $^{13}C^{33}H$ (64)
16	A′	3007	2905	3015	2915	vw	γ $^{11}C^{28}H$ (12), γ $^{11}C^{29}H$ (72)
17	A′	3002	2901	3013	2913	m	γ $^{10}C^{27}H$ (22), γ $^{10}C^{26}H$ (12), γ $^{12}C^{30}H$ (38), γ $^{12}C^{31}H$ (18), γ $^{13}C^{33}H$ (11), γ $^{13}C^{32}H$ (11)
18	A′	2997	2896	3006	2906	vw	γ $^{10}C^{27}H$ (62), γ $^{10}C^{26}H$ (26), γ $^{12}C^{31}H$ (10), γ $^{12}C^{30}H$ (31)
19	A′	2990	2889	2998	2898	w	γ $^{13}C^{32}H$ (78), γ $^{13}C^{33}H$ (14)
20	A′	1690	1633	1786	1727	vs	τ $^{15}O^{14}C$ (87)
21	A′	1643	1587	1641	1587	vw	τ $^{2}C^{4}C$ (10), τ $^{3}C^{5}C$ (30)
22	A′	1623	1568	1622	1568	vw	τ $^{4}C^{6}C$ (28), τ $^{1}C^{2}C$ (20)
23	A′	1542	1490	1525	1475	vw	α $^{19}H^{2}C^{4}C$ (16), α $^{20}H^{3}C^{5}C$ (18), α $^{22}H^{5}C^{6}C$ (18)
24	A′	1542	1490	1508	1458	vw	σ $^{29}H^{11}C^{28}H$ (27), σ $^{31}H^{12}C^{30}H$ (57)
25	A″	1534	1482	1498	1448	vw	δ $^{35}H^{17}C^{16}O^{14}C$ (10), δ $^{36}H^{17}C^{16}O^{14}C$ (10)
26	A′	1530	1479	1495	1445	vw	α $^{25}H^{9}N^{11}C$ (44), σ $^{27}H^{10}C^{26}H$ (11), σ $^{29}H^{11}C^{28}H$ (48), σ $^{31}H^{12}C^{30}H$ (12), δ $^{25}H^{9}N^{11}C^{13}C$ (11)
27	A′	1530	1478	1494	1444	vw	σ $^{33}H^{13}C^{32}H$ (24)
28	A′	1526	1474	1490	1440	vw	σ $^{27}H^{10}C^{26}H$ (53), σ $^{31}H^{12}C^{30}H$ (19), σ $^{33}H^{13}C^{32}H$ (17)
29	A′	1514	1463	1485	1436	vw	α $^{21}H^{4}C^{6}C$ (10), α $^{23}H^{6}C^{5}C$ (23)

30	A″	1509	1458	1483	1434	vw	δ $^{34}H^{17}C^{16}O^{14}C$ (18)
31	A′	1503	1452	1477	1428	vw	α $^{25}H^{9}N^{11}C$ (20), σ $^{27}H^{10}C^{26}H$ (23), σ $^{33}H^{13}C^{32}H$ (39)
32	A′	1478	1428	1468	1419	vw	ω $^{34}H^{17}C^{36}H$ (33), ω $^{35}H^{17}C^{34}H$ (38), ω $^{36}H^{17}C^{35}H$ (10)
33	A′	1422	1374	1405	1359	vw	α $^{18}H^{8}C^{9}N$ (40), α $^{28}H^{11}C^{13}C$ (15)
34	A″	1415	1367	1388	1342	vw	δ $^{24}H^{7}C^{14}C^{16}O$ (15), δ $^{29}H^{11}C^{9}N^{8}C$ (15), ω $^{29}H^{11}C^{28}H$ (11)
35	A″	1400	1353	1382	1336	vw	δ $^{18}H^{8}C^{9}N^{11}C$ (10), δ $^{27}H^{10}C^{12}C^{13}C$ (11), δ $^{30}H^{12}C^{13}C^{11}C$ (19), ω $^{29}H^{11}C^{28}H$ (10), ω $^{30}H^{12}C^{31}H$ (12)
36	A″	1397	1350	1376	1331	m	δ $^{18}H^{8}C^{9}N^{11}C$ (13), δ $^{29}H^{11}C^{9}N^{8}C$ (16), ω $^{29}H^{11}C^{28}H$ (14)
37	A″	1396	1349	1374	1328	vw	δ $^{32}H^{13}C^{12}C^{10}C$ (13), ω $^{26}H^{10}C^{27}H$ (14), ω $^{30}H^{12}C^{31}H$ (12), ω $^{32}H^{13}C^{33}H$ (13)
38	A″	1387	1340	1366	1321	vw	δ $^{26}H^{10}C^{12}C^{13}C$ (11), δ $^{27}H^{10}C^{12}C^{13}C$ (16), δ $^{31}H^{12}C^{13}C^{11}C$ (19), ω $^{32}H^{13}C^{33}H$ (14), ω $^{26}H^{10}C^{27}H$ (12)
39	A′	1375	1329	1354	1309	w	α $^{24}H^{7}C^{14}C$ (11), ω $^{26}H^{10}C^{27}H$ (14), ω $^{30}H^{12}C^{31}H$ (12), ω $^{32}H^{13}C^{33}H$ (11), ω $^{29}H^{11}C^{28}H$ (13)
40	A′	1360	1314	1348	1304	vw	τ $^{2}C^{4}C$ (10), τ $^{3}C^{5}C$(14), δ $^{24}H^{7}C^{14}C^{16}O$ (13), ω $^{32}H^{13}C^{33}H$ (12), ω $^{29}H^{11}C^{28}H$ (12)
41	A″	1331	1287	1317	1273	m	η $^{30}H^{12}C^{31}H$ (12), η $^{29}H^{11}C^{28}H$ (11)
42	A″	1321	1277	1308	1264	vw	α $^{28}H^{11}C^{13}C$ (25), δ $^{28}H^{11}C^{9}N^{8}C$ (11), η $^{30}H^{12}C^{31}H$ (12), η $^{29}H^{11}C^{28}H$ (10), η $^{32}H^{13}C^{33}H$ (10)
43	A″	1309	1265	1291	1248	vw	δ $^{27}H^{10}C^{12}C^{13}C$ (10), η $^{32}H^{13}C^{33}H$ (11), η $^{26}H^{10}C^{27}H$ (10)
44	A″	1273	1230	1258	1217	vw	δ $^{24}H^{7}C^{14}C^{16}O$ (21), δ $^{18}H^{8}C^{9}N^{11}C$ (12), η $^{29}H^{11}C^{28}H$ (10)
45	A″	1238	1196	1223	1183	m	δ $^{33}H^{13}C^{12}C^{10}C$ (14), η $^{32}H^{13}C^{33}H$ (14)
46	A″	1229	1188	1214	1174	w	δ $^{35}H^{17}C^{16}O^{14}C$ (11), δ $^{36}H^{17}C^{16}O^{14}C$ (10), η $^{32}H^{13}C^{33}H$ (12), η $^{34}H^{17}C^{35}H$ (14), η $^{34}H^{17}C^{36}H$ (11)
47	A′	1226	1185	1208	1168	vw	α $^{19}H^{2}C^{4}C$ (25), α $^{20}H^{3}C^{5}C$ (16), α $^{21}H^{4}C^{6}C$ (10), δ $^{35}H^{17}C^{16}O^{14}C$ (11), η $^{34}H^{17}C^{35}H$ (14), η $^{34}H^{17}C^{36}H$ (10)
48	A″	1211	1170	1207	1167	vw	δ $^{36}H^{17}C^{16}O^{14}C$ (11), η $^{34}H^{17}C^{35}H$ (13)
49	A′	1201	1160	1182	1143	vw	α $^{21}H^{4}C^{6}C$ (22), α $^{22}H^{5}C^{6}C$ (17), α $^{23}H^{6}C^{5}C$ (35)
50	A′	1197	1156	1178	1138	s	α $^{30}H^{12}C^{13}C$ (15), η $^{29}H^{11}C^{28}H$ (15), η $^{30}H^{12}C^{31}H$ (12)
51	A″	1175	1135	1171	1132	vs	α $^{24}H^{7}C^{14}C$ (12), ρ $^{34}H^{17}C^{36}H$ (15), ρ $^{35}H^{17}C^{34}H$ (13), δ $^{34}H^{17}C^{16}O^{14}C$ (36), δ $^{35}H^{17}C^{16}O^{14}C$ (16), δ $^{36}H^{17}C^{16}O^{14}C$ (17)
52	A′	1166	1127	1171	1132	vw	ρ $^{35}H^{17}C^{36}H$(70)
53	A″	1159	1120	1153	1115	vw	δ $^{18}H^{8}C^{9}N^{11}C$ (10), δ $^{31}H^{12}C^{13}C^{11}C$ (10), δ $^{10}C^{12}C^{13}C^{11}C$ (16), ρ $^{30}H^{12}C^{31}H$ (10), ρ $^{32}H^{13}C^{33}H$ (10)
54	A′	1128	1090	1119	1082	w	τ $^{9}N^{11}C$ (25), τ $^{9}N^{8}C$ (26), τ $^{10}C^{12}C$ (10), η $^{32}H^{13}C^{33}H$ (11)
55	A′	1111	1074	1102	1065	vw	τ $^{2}C^{4}C$ (19), α $^{20}H^{3}C^{5}C$ (10), α $^{23}H^{6}C^{5}C$ (14)
56	A″	1087	1050	1069	1033	vw	δ $^{31}H^{12}C^{13}C^{11}C$ (10)
57	A′	1061	1025	1053	1018	vw	τ $^{4}C^{6}C$ (17), τ $^{5}C^{6}C$ (21), α $^{22}H^{5}C^{6}C$ (10), α $^{3}C^{5}C^{6}C$ (11)
58	A″	1059	1023	1049	1014	vw	δ $^{33}H^{13}C^{12}C^{10}C$ (10)
59	A′	1037	1002	1030	995	vw	τ $^{14}C^{7}C$ (13), τ $^{16}O^{17}C$ (21)
60	A′	1034	999	1022	988	w	τ $^{13}C^{11}C$ (16), τ $^{16}O^{17}C$ (12), α $^{11}C^{9}N^{8}C$ (16), α $^{13}C^{11}C^{9}N$ (11)
61	A′	1030	995	1018	984	vw	τ $^{5}C^{6}C$ (11), α $^{2}C^{4}C^{6}C$ (14), α $^{3}C^{5}C^{6}C$ (27), α $^{5}C^{6}C^{4}C$ (17)
62	A″	1017	983	1005	971	vw	δ $^{20}H^{3}C^{1}C^{7}C$ (12), δ $^{21}H^{4}C^{2}C^{1}C$ (11), δ $^{22}H^{5}C^{6}C^{4}C$ (24), δ $^{23}H^{6}C^{5}C^{3}C$ (21), δ $^{3}C^{5}C^{6}C^{4}C$ (12)
63	A″	1010	976	988	955	vw	δ $^{19}H^{2}C^{1}C^{7}C$ (17), δ $^{20}H^{3}C^{1}C^{7}C$ (21), δ $^{21}H^{4}C^{2}C^{1}C$ (26), δ $^{22}H^{5}C^{6}C^{4}C$ (11)
64	A′	983	949	986	953	vw	τ $^{16}O^{17}C$ (16), τ $^{8}C^{7}C$ (20)
65	A′	960	928	952	920	vw	τ $^{16}O^{17}C$ (12)
66	A″	941	910	932	901	vw	δ $^{19}H^{2}C^{1}C^{7}C$ (19), δ $^{20}H^{3}C^{1}C^{7}C$ (16), δ $^{23}H^{6}C^{5}C^{3}C$ (15)
67	A′	903	872	909	879	vw	τ $^{10}C^{12}C$ (13)
68	A″	890	860	895	865	vw	θ $^{15}O^{7}C^{16}O^{14}C$ (14)
69	A″	883	853	879	850	vw	δ $^{33}H^{13}C^{12}C^{10}C$ (11)
70	A′	879	850	870	841	vw	δ $^{33}H^{13}C^{12}C^{10}C$ (10)
71	A″	866	837	857	829	vw	δ $^{19}H^{2}C^{1}C^{7}C$ (27), δ $^{20}H^{3}C^{1}C^{7}C$ (22), δ $^{21}H^{4}C^{2}C^{1}C$ (22), δ $^{22}H^{5}C^{6}C^{4}C$ (27)
72	A″	833	805	824	796	vw	δ $^{32}H^{13}C^{12}C^{10}C$ (11)
73	A″	819	792	815	788	vw	δ $^{32}H^{13}C^{12}C^{10}C$ (11)
74	A′	786	759	788	762	vw	α $^{15}O^{14}C^{16}O$(17)
75	A″	740	715	744	719	w	δ $^{21}H^{4}C^{2}C^{1}C$ (11), θ $^{15}O^{7}C^{16}O^{14}C$ (15)
76	A″	730	705	725	701	vw	β $^{15}O^{14}C^{16}O$ (15), θ $^{15}O^{7}C^{16}O^{14}C$ (15)
77	A″	713	689	713	689	w	δ $^{23}H^{6}C^{5}C^{3}C$ (25), δ $^{3}C^{5}C^{6}C^{4}C$ (11), δ $^{1}C^{2}C^{4}C^{6}C$ (23), θ $^{7}C^{3}C^{2}C^{1}C$ (11)

78	A″	655	633	706	683	s	δ $^{25}H^{9}N^{11}C^{13}C$ (39)
79	A′	641	620	641	620	vw	α $^{2}C^{4}C^{6}C$ (11), α $^{11}C^{9}N^{8}C$ (12)
80	A′	616	595	629	608	vw	α $^{1}C^{2}C^{4}C$ (12), α $^{2}C^{4}C^{6}C$ (24), α $^{3}C^{5}C^{6}C$ (15)
81	A′	581	562	607	587	vw	α $^{1}C^{2}C^{4}C$ (17)
82	A″	529	512	519	501	vw	δ $^{22}H^{5}C^{6}C^{4}C$ (11), δ $^{3}C^{5}C^{6}C^{4}C$ (11), θ $^{7}C^{3}C^{2}C^{1}C$ (30)
83	A′	497	480	497	480	vw	α $^{12}C^{13}C^{11}C$ (20), α $^{13}C^{11}C^{9}N$ (21)
84	A′	452	437	454	439	vw	β $^{12}C^{13}C^{11}C$ (23)
85	A′	441	426	447	433	vw	β $^{12}C^{13}C^{11}C$ (23)
86	A″	427	412	416	402	vw	δ $^{21}H^{4}C^{2}C^{1}C$ (11), δ $^{2}C^{4}C^{6}C^{5}C$ (33), δ $^{3}C^{5}C^{6}C^{4}C$ (36)
87	A″	364	352	367	355	vw	β $^{16}O^{14}C^{7}C$ (10), β $^{17}C^{16}O^{14}C$ (17), δ $^{10}C^{12}C^{13}C^{11}C$ (10)
88	A″	357	345	358	346	vw	β $^{9}N^{8}C^{7}C$ (12), δ $^{11}C^{9}N^{8}C^{7}C$ (10), δ $^{13}C^{11}C^{9}N^{8}C$ (16)
89	A′	341	330	345	333	vw	α $^{15}O^{14}C^{16}O$ (14), α $^{7}C^{1}C^{2}C$ (15)
90	A′	281	272	283	274	vw	β $^{16}O^{14}C^{7}C$ (10), β $^{7}C^{1}C^{2}C$ (21), β $^{17}C^{16}O^{14}C$ (30)
91	A′	260	251	260	251	vw	α $^{16}O^{14}C^{7}C$ (11)
92	A″	253	244	250	242	vw	δ $^{2}C^{4}C^{6}C^{5}C$ (13), δ $^{12}C^{13}C^{11}C^{9}N$ (20)
93	A″	219	211	217	210	vw	δ $^{17}C^{16}O^{14}C^{7}C$ (25)
94	A″	178	172	180	174	vw	β $^{9}N^{8}C^{7}C$ (10), δ $^{34}H^{17}C^{16}O^{14}C$ (10), δ $^{13}C^{11}C^{9}N^{8}C$ (13), δ $^{17}C^{16}O^{14}C^{7}C$ (30)
95	A″	160	155	163	158	vw	β $^{16}O^{14}C^{7}C$ (11), β $^{7}C^{1}C^{2}C$ (17), θ $^{14}C^{8}C^{1}C^{7}C$ (20)
96	A″	125	121	143	138	vw	β $^{14}C^{7}C^{1}C$ (11), δ $^{34}H^{17}C^{16}O^{14}C$ (22), δ $^{35}H^{17}C^{16}O^{14}C$ (17), δ $^{36}H^{17}C^{16}O^{14}C$ (20)
97	A″	100	96	112	108	vw	β $^{14}C^{7}C^{1}C$ (22), δ $^{16}O^{14}C^{7}C^{8}C$ (19), δ $^{17}C^{16}O^{14}C^{7}C$ (19)
98	A″	91	88	90	87	vw	β $^{9}N^{8}C^{7}C$ (14), δ $^{11}C^{9}N^{8}C^{7}C$ (45), θ $^{14}C^{8}C^{1}C^{7}C$ (24)
99	A″	79	76	80	77	vw	β $^{8}C^{7}C^{1}C$ (35), θ $^{7}C^{3}C^{2}C^{1}C$ (17)
100	A″	52	50	52	51	vw	δ $^{16}O^{14}C^{7}C^{8}C$ (17), δ $^{9}N^{8}C^{7}C^{1}C$ (31), δ $^{8}C^{7}C^{1}C^{3}C$ (29)
101	A″	45	43	44	43	vw	δ $^{9}N^{8}C^{7}C^{1}C$ (10), δ $^{8}C^{7}C^{1}C^{3}C$ (59), θ $^{7}C^{3}C^{2}C$ ^{1}C (11)
102	A″	27	26	30	29	vw	δ $^{16}O^{14}C^{7}C^{8}C$ (35), δ ^{9}N ^{8}C ^{7}C ^{1}C (46)

S^{y}, symmetry; τ, stretching; γ, symmetric stretching; ϕ, asymmetric stretching; α, in-plane bending; β, out-of-plane bending; δ, torsion; σ, Scissoring; ω, wagging; η, twisting; ρ, rocking; θ, out; vw, very weak; w, weak; m, medium; s, strong; vs, very strong.

Analysis of benzene ring

Aromatic CH stretching vibrations: The aromatic organic compounds typically show the presence of stretching vibrations in the region of 3100-3000 cm^{-1} [42,43]. It is the characteristic region for identifying CH stretching vibrations. For the title molecule, 3089, 3080, 3069, 3059 and 3052 cm^{-1} are assigned to aromatic CH stretching vibrations. The aromatic CH bending vibrations (both in-plane and out-of-plane) are generally observed as several strong to weak bands in the region of 1300-1000 cm^{-1} and 1000-750 cm^{-1} [44-50]. The bands for in-plane bending are observed at 1475, 1436, 1167, 1143, 1065 and 1018 cm^{-1}. The frequencies 971, 955, 901, 829, 719, 689, 501 and 402 cm^{-1} are due to the aromatic CH out-of-plane bending vibrations. Except some vibrations, all the bending vibrations agree well with the literature. Some bending vibrations are deviate slightly from the expected region since the calculation is conducted in the gaseous state.

Aromatic C=C vibrations: Generally, the aromatic C=C stretching vibrations are appeared in the region of 1650-1430 cm^{-1} [51]. The six aromatic carbon atoms undergo coupled vibrations (skeletal vibrations) to produce a maximum of four bands in the region of 1660-1420 cm^{-1}. As per the previous literature [52], the main peaks at 1587, 1568 and 1304 cm^{-1} are due to strong C=C stretching and the vibrations at 1065, 1018 and 984 cm^{-1} are assigned to the skeletal vibrations of the benzene ring of the title molecule. The aromatic CCC in-plane bending vibrations are appeared at 1018, 984, 608, 620 and 587 cm^{-1}. The aromatic CCCC torsion vibrations are observed at 971, 501, 402 and 242 cm^{-1}. Except for some vibrations, all the stretching vibrations are coherent with the literature [53].

Analysis of piperidine ring

C–C stretching: The C–C stretching frequencies of aliphatic ring are observed at 1082, 995, 988, 953 and 879 cm^{-1}.

NH stretching vibration: The –NH stretching peaks of the aliphatic ring (piperidine) are observed at 3364 cm^{-1} [54]. For the molecule under investigation, the band appeared at 3415 cm^{-1}.

Other vibrations: The computed stretching frequency of C-N is located at 1082 cm^{-1} for the investigated molecule. The bending (in-plane) vibrations of HCN are appeared at 1445 and 1428 cm^{-1}, whereas the bending (out-plane) vibration of NCC is observed at 174 cm^{-1}. The CCN in-plane bending peaks are recognized at 988 and 480 cm^{-1}. The CNC in-plane bending vibrations are spotted at 988 and 620 cm^{-1}. The torsion type of vibrations for CCCN (242 cm^{-1}), CCNC (346, 174 cm^{-1}), CNCC (346, 87 cm^{-1}), HNCC (683 cm^{-1}), NCCC (51, 43 and 29 cm^{-1}) and HCNC (1336, 1342, 1331, 1264, 1217 and 1115 cm^{-1}) are also observed at the positions as provided in the parenthesis.

CH_2 vibrations: Six patterns of vibrations are possible for the $–CH_2$ moiety, namely symmetric stretching, asymmetric stretching, scissoring, rocking vibrations (in-plane-A′), wagging and twisting (out-of-plane-A″) vibrations. The CH stretching of the methylene groups is observed at lower frequencies than the aromatic CH frequencies [55]. The stretching vibrations

of CH are seen at 2991 and 2961 cm^{-1}, whereas the asymmetric CH_2 vibrations are appeared in the region of 3000-2900 cm^{-1} [55]. The asymmetric stretching vibrations are located at 2968, 2963, 2952 and 2945 cm^{-1} as medium and weak bands for the title molecule.

The CH symmetric stretching vibrations appeared between 2900 and 2800 cm^{-1} [56,57]. For the title molecule, the symmetrical stretching vibrations are observed at 2968, 2945, 2915, 2913, 2906 and 2898 cm^{-1}. The bending vibrations are usually seen in between 1500-800 cm^{-1}. For the title molecule, the scissoring vibrations are monitored at 1458, 1445, 1444, 1440 and 1428 cm^{-1}. The rocking type of vibrations are placed at 1115 cm^{-1}. The wagging vibrations are appeared at 1342, 1336, 1331, 1328, 1321, 1309 and 1304 cm^{1}. The twisting vibrations are found at 1273, 1264, 1248, 1217, 1183, 1174, 1168, 1167, 1138 and 1082 cm^{-1}.

The HCC in-plane bending vibrations are grasped at 1359, 1273, 1264 and 1138 cm^{-1}. The CCC in-plane bending of the piperidine ring is identified at 480 cm^{-1}, while the out-of-plane bending vibrations are experienced at 439 and 433 cm^{-1}. The torsion HCCC type of vibrations are generated at 1336, 1328, 1321, 1248, 1183, 1115, 1033, 1014, 850, 841, 796 and 788 cm^{-1}.

Methyl group vibrations: Generally, the CH stretching in alkanes occurs at lower frequencies than those of the aromatic rings (3150-3050 cm^{-1}). The CH_3 stretching vibrations are expected at 2980-2870 cm^{-1} [58] as weak bands. For title molecule, the peak appears at 2949 cm^{-1} and the symmetric stretching vibrations appear at 3042 cm^{-1} [59]. Similarly, the asymmetric CH vibrations are established at 3049 and 3020 cm^{-1}. The twisting mode of vibrations was detected at 1174, 1169 and 1168 cm^{-1}. The wagging mode of vibration is positioned at 1419 cm^{-1} and the peaks at 1448 and 1434 cm^{-1} are due to the scissoring mode of vibrations.

Ester group vibrations

C=O and C-O vibrations: The C=O stretching vibration is generally pointed at 1789 cm^{-1} and in case of the title molecule, this vibration is located at 1727 cm^{-1}. The C-O stretching frequencies are observed at 1132, 995, 988, 953 and 920 cm^{-1}. The in-plane bending vibration of COC is observed at 251 cm^{-1}. The out-plane bending vibrations of COC are appeared at 355, 274 and 158 cm^{-1}, while the in-plane bending vibrations of OCO vibrations are observed at 763 and 333 cm^{-1}. The out type of vibrations are recognized at 865, 719 and 701 cm^{-1} as weak signals. The torsion COCC type of vibrations are detected at 210, 174 and 108 cm^{-1}, whereas the torsion HCCO vibrations are appeared at 1342, 1304 and 1217 cm^{-1}. The signals at 1448, 1434, 1174, 1168, 1167, 1132, 174 and 138 cm^{-1} are due to the torsion HCOC vibrations. The signals at 108, 51 and 29 cm^{-1} are appeared due to the torsion vibrations of OCCC, whereas the OCC out-of-plane bending vibration is recognized at 355 cm^{-1}.

Vibration of bridge atom: The atom C7 is a centre bridge that connects the aromatic benzene ring, piperidine and acetyl group. The bending (in-plane) CCC vibrations are appeared to be at 865 and 333 cm^{-1}. The signals at 1376 and 1309 cm^{-1} are due to in-plane bending HCC vibration. The out-of-plane CCC vibrations are seen at 274, 158, 138, 108 and 77 cm^{-1}. The NCC out-of-plane bending vibrations are appeared at 346 and 87 cm^{-1}. The signals at 689, 501, 158, 87, 77 and 43 cm^{-1} are due to CCCC out-plane vibrations. The torsion CCCC vibrations occurred at 51 and 45 cm^{-1} as weak signals.

Second-order perturbation theory: The chemical explanation of hyperconjugative interaction and electron density transfer (EDT) from filled lone electron pairs of the n(Y) of the "Lewis base" Y into the unfilled anti-bond σ*(X–H) of the "Lewis acid" X-H in systems of X-HY hydrogen bonding systems have been successfully demonstrated by the NBO analysis [60,61]. The stabilization energy $E_{(2)}$ associated with i–j delocalization is computed for each donor (i) and acceptor (j) as follows:

$$E_2 = \Delta E_{i,j} = q_i \frac{F(i,j)^2}{\varepsilon_j - \varepsilon_i} \quad (13)$$

where q_i is the donor orbital occupancy, E_i and E_j are the diagonal elements and F(i,j) is the off-diagonal NBO Fock matrix element. The larger the $E_{(2)}$ value, the more intensive the interaction between electron-donating and electron-accepting groups [62,63]. The NBO analysis for the target molecule was determined under the B3LYP/6-311++G(d,p) basis set.

For this molecule, σ→σ*, π→π*, LP→σ* and LP→π* interactions are reported selectively in Table-11. The transition from the donor-acceptor systems, *viz.* σ(C7 - H24)→σ*(C1-C3), σ(C2-H19)→σ*(C1-C3), σ(C3-H20)→σ*(C1-C2) and σ(C7-H24)→σ*(C14-O15), is helpful for the stabilization of the molecule with energies of 4.70, 4.72, 4.73 and 4.94 kcal/mol, respectively. The donors like π(C3-C5), π(C1-C2) and π(C3-C5) donate electrons to the acceptor systems, *viz.* π*(C4-C6), π*(C4-C6) and π*(C1-C2), with energies of 20.56, 20.70 and 21.26 kcal/mol, respectively. These transitions are helpful for the stabilization of the molecule. The energies of 7.19, 7.38 and 7.88 kcal/mol are due to the transitions from LP(1) N9→σ*(C8-C10), LP(1) N9→σ*(C11-C13) and LP(1) O16→σ*(C14-O15), respectively, thus enhancing the stability of the molecule. The electronic transitions from LP(2) O15→σ*(C7-C10) and LP(2) O15→σ*(C14–O16) respectively, are greatly responsible for the stabilization with energies of 18.06 and 32.86 kcal/mol, respectively. The LP(2) O16→π*(C14-O15) is helpful to stabilize the molecule with energy 47.44 kcal/mol. The other transitions are also helpful for the stabilization of the molecule.

NLO analysis: The first-order hyperpolarizability of the molecule was studied with the help of B3LYP/6-311++G(d,p) method. Also, the related physical properties like dipole moment, mean polarizability, anisotropy of polarizability and vector component were also calculated. When an applied field is present, a system's energy is regarded as a function of the electric field. The first-order hyperpolarizability is the third-rank tensor that is represented by 3 × 3 × 3 matrices. In total, 27 components of the 3D matrix can be reduced to 10 components according to Kleinman symmetry [64]. The dipole moment, anisotropy of polarizability, mean polarizability, first hyperpolarizability and B_{vec} using XYZ [24,65] components are defined as follows:

TABLE-11
SECOND-ORDER PERTURBATION THEORY ANALYSIS OF FOCK MATRIX IN NBO BASIC CORRESPONDING TO THE INTERMOLECULAR BONDS OF THE TARGET MOLECULE

S. No.	Type	Donor NBO	ED/e (a.u.)	Type	Acceptor NBO	ED/e (a.u.)	E(2) (kcal/mol)	E(j)-E(i) (a.u.)	F(i,j) (a.u.)
1	π	C1-C2	1.66159	π*	C3-C5	0.31688.	19.53	0.29	0.067
2	π	C1-C2	1.66159	π*	C4-C6	0.33252	20.70	0.28	0.068
3	σ	C2-H19	1.97959	σ*	C1-C3	0.02592	4.72	1.09	0.064
4	π	C3-C5	1.66170	π*	C1-C2	0.35039	21.26	0.28	0.070
5	π	C3-C5	1.66170	π*	C4-C6	0.33252	20.56	0.28	0.068
6	σ	C3-H20	1.97827	σ*	C1-C2	0.02329	4.73	1.09	0.064
7	π	C4-C6	1.66859	π*	C1-C2	0.35039	19.89	0.29	0.068
8	π	C4-C6	1.66859	π*	C3-C5	0.31688	19.92	0.29	0.068
9	σ	C7-C14	1.96305	σ*	O16-C17	0.01839	4.18	0.89	0.055
10	σ	C7-H24	1.97028	σ*	C1-C3	0.02592	4.70	1.07	0.063
11	σ	C7-H24	1.97028	σ*	C14-O15	0.02285	4.94	1.11	0.066
12	σ	C8-H18	1.98909	σ*	N9-C11	0.01872	4.05	0.85	0.053
13	σ	C10-H26	1.97740	σ*	C 8-N9	0.02492	4.05	0.84	0.052
14	LP(1)	N9	1.91756	σ*	C 8-C10	0.03196	7.19	0.66	0.062
15	LP(1)	N9	1.91756	σ*	C11-C13	0.02710	7.38	0.67	0.064
16	LP(2)	O15	1.84344	σ*	C 7-C14	0.06743	18.06	0.64	0.098
17	LP(2)	O15	1.84344	σ*	C14-O16	0.10390	32.86	0.63	0.130
18	LP(1)	O16	1.96344	σ*	C14-O15	0.02285	7.88	1.18	0.086
19	LP(2)	O16	1.78704	π*	C14-O15	0.21661	47.44	0.34	0.114
20	LP(2)	O16	1.78704	σ*	C17-H35	0.01315	4.63	0.72	0.054
21	LP(2)	O16	1.78704	σ*	C17-H36	0.01322	4.50	0.71	0.053

'E(2) is the energy of hyperconjugative interaction (stabilization energy); E(j)-E(i) is the energy difference between donor and acceptor i and j NBO orbitals; F(i,j) is the Fock matrix element between i and j NBO orbitals; ED/e is the electron density of donor and acceptor NBO orbitals; LP(n)A is a valence lone pair orbital (n) on A atom'

$$\mu = \sqrt{\mu_x^2 + \mu_y^2 + \mu_z^2} \quad (14)$$

$$\alpha = \frac{\alpha_{xx} + \alpha_{yy} + \alpha_{zz}}{3} \quad (15)$$

$$\alpha = \frac{1}{\sqrt{2}}\sqrt{(\alpha_{xx} - \alpha_{yy})^2 + (\alpha_{yy} - \alpha_{zz})^2 + (\alpha_{zz} - \alpha_{xx})^2 + 6\alpha_{xx}^2} \quad (16)$$

$$\beta_{Tot} = \sqrt{\beta_x^2 + \beta_y^2 + \beta_z^2} \quad (17)$$

where

$$\beta_x = \beta_{xxx} + \beta_{xyy} + \beta_{xzz} \quad (18)$$

$$\beta_y = \beta_{yyy} + \beta_{xxy} + \beta_{yzz} \quad (19)$$

$$\beta_z = \beta_{zzz} + \beta_{xxz} + \beta_{yyz} \quad (20)$$

$$\beta_{vec} = \frac{3}{5}\sqrt{(\beta_{xxx} + \beta_{xyy} + \beta_{xzz})^2 + (\beta_{yyy} + \beta_{xxy} + \beta_{yzz})^2 + (\beta_{zzz} + \beta_{xxz} + \beta_{xyz})^2} \quad (21)$$

The molecule's dipole moment is theoretically calculated as 0.8101 D. The highest value is in the μ_Z direction (0.3956 D) and the highest static polarizability is located on α_{xx} (207.511 a.u.). The highest static first order hyperpolarizability is placed on β_{xxx} (145.6128 a.u.).

The α, μ and β values are computed from Gaussian 16W software and tabulated as atomic units in Table-12. The predicted values are converted into e.s.u. units and the conversion factors are given below [66]:

α: 1 a.u. = 0.1482×10^{-24} e.s.u.
β: 1 a.u. = 8.6393×10^{-33} e.s.u

TABLE-12
THE MEAN POLARIZABILITY Δα (e.s.u.), ANISOTROPY OF POLARIZABILITY α (e.s.u.), DIPOLE MOMENT μ (Debye) AND FIRST HYPERPOLARIZABILITY β_{Tot} (e.s.u.) AND VECTOR COMPONENT β_{Vec} (e.s.u.) DETERMINATIONS FOR THE TARGET MOLECULE

Dipole-moment (D)		Static first order hyper-polarizability (a.u.)	
μ_x	-0.4752	β_{xxx}	145.6128
μ_y	-0.5234	β_{xxy}	-21.6069
μ_z	0.3956	β_{xyy}	8.0781
μ (Debye)	0.8101	β_{yyy}	20.4462
Static polarizability (a.u.)		β_{xxz}	28.0654
α_{xx}	207.511	β_{xyz}	30.6052
α_{xy}	-9.7661	β_{yyz}	14.3452
α_{yy}	164.1814	β_{xzz}	-26.5872
α_{xz}	-5.2469	β_{yzz}	-74.29
α_{yz}	-9.6006	β_{zzz}	23.9113
α_{zz}	155.8308		
α_{Tot} (a.u.)	175.8411	β_{Tot} (a.u.)	162.0085
α_{Tot} (e.s.u)	0.2606×10^{-24}	β_{Tot} (e.s.u)	1.3996×10^{-30}
Δα (a.u.)	465.2250	β_{Vec} (a.u.)	97.2050
Δα (e.s.u)	0.0534×10^{-24}	β_{Vec} (e.s.u.)	8.3971×10^{-31}

Since the values of the polarizabilities (α) and first-order hyperpolarizability (β) of the G 16W output are in atomic units (a.u.) and converted into electrostatic units (e.s.u.), α: 1 a.u. = 0.1482×10^{-24} e.s.u.; β : 1 a.u. = 8.6393×10^{-33} e.s.u.)

The calculated μ_{Tot}, Δα, α_{Tot}, β_{Tot} and β_{vec} values are also given in Table-12. The μ_{Tot}, α_{Tot} and β_{Tot} values are found to be 0.8101D, 0.2606×10^{-24} e.s.u. and 1.3996×10^{-30} e.s.u., respec-

TABLE-13
DOCKING SCORE AND XYZ ORIENTATION OF DOCKING OF LIGANDS WITH 7ZHA

Ligand representation	Binding energy (kcal/mol)	X	Y	Z
Compound **A***	–	114.930280	114.911800	118.759880
Compound **A**$^{\#}$	-11.4	113.082120	116.559400	119.297040
Dexmethylphenidate	-7.5	110.451445	115.084888	119.940445
Compound **1**	-6.4	104.901789	104.448106	106.656053
Compound **2**	-6.2	120.585761	109.271000	117.344810
Compound **3**	-6.1	119.681100	109.461499	117.925950
Compound **4**	-8.3	111.047736	115.793105	120.452842
Compound **5**	-7.5	111.081095	115.142715	119.853714
Compound **6**	-7.8	110.230350	114.484949	120.218850
Compound **7**	-7.8	110.947264	115.754052	119.980525
Compound **8**	-8.0	110.613095	114.155238	120.521476
Compound **9**	-7.8	110.529200	114.350101	120.425550

*downloaded, unprepared protein 7ZHA's heteroatom; #the same, energy minimized ligand binding with the prepared protein 7ZHA

tively. It is found that the β_{Tot} is 3.7 times greater than urea. (Urea μ_{Tot} = 1.3732D, $\beta_{Tot} = 0.3728 \times 10^{-30}$ e.s.u.) [67].

Structure-activity relationship: Dexmethylphenidate is a drug used for attention deficit the hyperactivity disorder. Its mechanism of action explains that it binds with the 7ZHA protein in homo sapiens. The PDB structure of the protein 7ZHA is downloaded from the RCSB website (https://www.rcsb.org/structure/7ZHA).

Preparation of protein: Discovery studio visualizer helps in the preparation of the downloaded protein. The heteroatoms and water molecules are removed from the protein. The force-field and partial charge applied were CHARMm and Momany-Rone, respectively. The quality of the prepared protein is checked with the help of the online tool SAVES (https://saves.mbi.ucla.edu/). The Ramachandran plot [68] shows that the percentage of residues in the allowed region is found to be 93.2%. Since the value is significant, it is decided to continue with the prepared protein, 7ZHA.

Ligand preparation: The 2D structure of dexmethylphenidate and its modified structures were drawn virtually with the help of the Chemsketch tool. They are saved as .pdb format files after being energy minimized with the help of Avogadro software. MMFF9 force field is applied and the algorithm selected is the steepest descent algorithm. The energy minimization is essential for the docking process. It reduces the computational time and produces the correct result. Fig. 14 shows the various structures selected for the SAR activity.

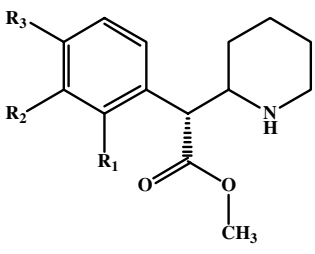

Compd. No.	R_1	R_2	R_3
1	CH_3	H	H
2	NH_2	H	H
3	OH	H	H
4	H	CH_3	H
5	H	NH_2	H
6	H	OH	H
7	H	H	CH_3
8	H	H	NH_2
9	H	H	OH

Fig. 14. Derived structures selected for SAR activity

Docking: The prepared protein and the energy-minimized ligands are docked with the help of the PyRx software. The binding energy for all the selected ligands and dexmethylphenidate, along with the XYZ orientation of docking are shown in Table-13. The heteroatom was used to crystallize the protein 7ZHA is found to be 1-ethyl-2-[(1-ethylquinolin-2-yl)methyl]-quinoline (compound **A***). The orientation of docking of ligand in the XYZ direction of the downloaded raw ligand (compound **A***) with protein 7ZHA is found to be 114.930280, 114.911800 and 118.759880, respectively. The same ligand is then energy minimized (compound **A**$^{\#}$) and docked with the prepared 7ZHA protein and its docking score is found to be -11.4 kcal/mol. Now, the XYZ orientations of docking have also been noticed. There is no major change in the XYZ orientation. Similarly, the patterns of all the XYZ orientations of docking for compounds **1-9** are almost in line with the raw ligand docked with the protein 7ZHA, except for compounds **1**, **2** and **3**.

The binding value for dexmethylphenidate with 7ZHA is found to be -7.5 kcal/mol. Compounds **4** (-8.3 kcal/mol) and **8** (-8.0 kcal/mol) have significant scores. The SWISS ADME properties of the compounds dexmethylphenidate, **4** and **8** are obtained and listed in Table-14, obey all the rules like Lipinski, Ghose, Veber, Egan, Muegge, *etc.*

TABLE-14
SWISS ADME RESULTS OBTAINED FOR DEXMETHYLPHENIDATE, COMPOUND **4** AND **8**

Properties	Dexmethylphenidate	Compd. **4**	Compd. **8**
Lipinski	Yes	Yes	Yes
Ghose	Yes	Yes	Yes
Veber	Yes	Yes	Yes
Egan	Yes	Yes	Yes
Muegge	Yes	Yes	Yes
BBB permeant	Yes	Yes	Yes

The docking patterns of raw ligand, dexmethylphenidate and compounds **4** and **8** were analyzed by Discovery Studio Visualizer and the interactions are shown in Table-15. The pattern of the docking is also shown in Fig. 15. Table-15 shows that all the small molecules (dexmethylphenidate, compound **4** and compound **8**) are docked with GLN A: 247 amino acid residue. The compound **8** establishes four hydrogen bonds with the protein 7ZHA. All the amino acid residues involved in docking are present in the active sites, according to the CASTp tool prediction of active binding sites.

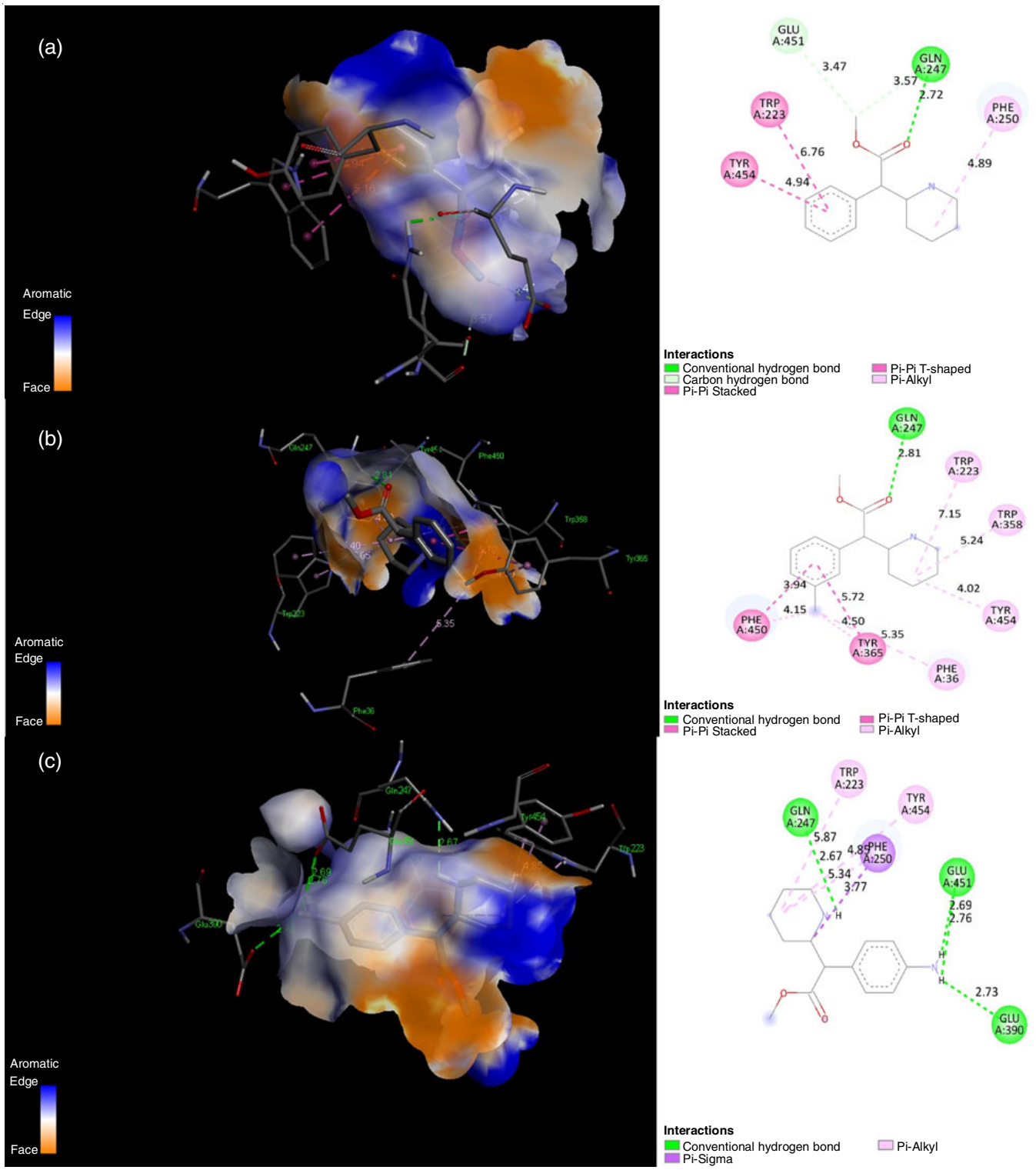

Fig. 15. Docking pattern of various ligands (a) dexmethylphenidate (b) compound **4** (c) compound **8** with protein 7ZHA

Conclusion

Dexmethylphenidate is a drug used in the treatment of attention deficit hyperactivity disorder. Using Gaussian 16W, all the experiments were performed in the gaseous state at the 311++G(d,p) level of theory. The electronic structure values like bond angle, bond distance and dihedral angles are well-matched in the earlier report. According to Mulliken population analysis, 1C has a higher positive value. The ESP study reveals that the molecule is susceptible to electrophilic attack. The frontier molecular orbital analysis expresses that this molecule is hard and stable. This molecule possesses both steric and van der Waals force of attractions as demonstrated by studies of the non-covalent interaction (NCI). Hole electron transfer analysis explains that at the S0→S1 excitation state, it follows

TABLE-15
DOCKING PATTERN OF VARIOUS LIGANDS AND PROTEIN 7ZHA

Compound	Interacting atom	Interacting amino acid	Hydrogen bond distance (Å)
Dexmethylphenidate	O	GLN A: 247	2.72
Compound **4**	O	GLN A: 247	2.81
Compound **8**	-N-H	GLN A: 247	2.67
	-N-H	GLU A: 451	2.76
	-N-H	GLU A: 451	2.69
	-N-H	GLU A: 390	2.73

$\pi \rightarrow \pi^*$ transition and charge transfer type is possible at the S0→S5 excitation level. The heat map investigation predicts that the electrons are richer in benzene at the S0→S1 excitation. The PDI, FLU, HOMA and Bird aromaticities were calculated and compared for benzene, toluene and DMP molecules. The STM analysis envisages that at V = -3.5 and Z = 2.2 Å conditions, the 'I' signal is more prominent almost over the molecule except for the CH_3 group attached to the ester group. A shaded surface map with a projection of localized orbital locator (LOL) enlightens that this molecule has electron-rich and electron-depleted domains. A simulated UV-Vis spectral analysis for the title compound was carried out in various solvents. Fukui function analysis was also performed. A simulated vibrational frequency study was also completed to understand the various types of vibrations better. The second-order perturbation theory describes that this molecule is very stable due to the participation of donor and acceptor systems available in the molecule, SAR activity analysis is also carried out.

ACKNOWLEDGEMENTS

The authors thank Management of St. John's College, Palayamkottai, India for providing the software facility.

CONFLICT OF INTEREST

The authors declare that there is no conflict of interests regarding the publication of this article.

REFERENCES

1. Diagnostic and Statistical Manual of Mental Disorders, American Psychiatric Publishing: Arlington, USA, edn 5, p. 59 (2013).
2. Diagnostic and Statistical Manual of Mental Disorders, Text Revision (DSM-5-TR), American Psychiatric Publishing, Washington D.C., edn 5 (2022).
3. D.M. Foreman, *Arch. Dis. Child.*, **91**, 192 (2005); https://doi.org/10.1136/adc.2004.064576
4. T.E. Brown, *Curr. Psychiatry Rep.*, **10**, 407 (2008); https://doi.org/10.1007/s11920-008-0065-7
5. S.V. Faraone and H. Larsson, *Mol. Psychiatry*, **24**, 562 (2019); https://doi.org/10.1038/s41380-018-0070-0
6. M.D. Moen and S.J. Keam, *CNS Drugs*, **23**, 1057 (2009); https://doi.org/10.2165/11201140-000000000-00000
7. T. van Mourik, M. Bühl and M.P. Gaigeot, *Philos. Trans.- Royal Soc., Math. Phys. Eng. Sci.*, **372**, 20120488 (2014); https://doi.org/10.1098/rsta.2012.0488
8. ACD/Chemsketch, 2017.2.1, Advanced Chemistry Development, Inc. (ACD/Labs), Oronto, ON, Canada (2017).
9. M.D. Hanwell, D.E. Curtis, D.C. Lonie, T. Vandermeersch, E. Zurek and G.R. Hutchison, *J. Cheminform.*, **4**, 17 (2012); https://doi.org/10.1186/1758-2946-4-17
10. M.J. Frisch, G.W. Trucks, H.B. Schlegel, G. E. Scuseria, M.A. Robb, J.R. Cheeseman, G. Scalmani, V. Barone, G.A. Peterson, H. Nakatsuji, X. Li, M. Caricato, A.V. Marenich, J. Bloino, B.G. Janesko, R.Comperts, B. Mennucci, H.P. Hratchian, J.V.Oritz, A.F. Izmaylov, J.L. Sonnenberg, D. Williams-Young, F. Ding, F. Lipparini, F.Egidi, J. Goings, B. Peng, A. Petrone, T. Henderson, D. Ranasinghe, V.G. Zakrzewski, J. Gao, N. Rega, G. Zheng, W. Liang, M. Hada, M. Ehara, K. Toyota, R. Fukuda, J. Hasegawa, M. Ishida, T. Nakajima, Y. Honda, O. Kitao, H. Nakai, T. Vereven, K. throssell, J.A.Montgomery, Jr., J.E. Peralta, F. Ogliaro, M.J. Bearpark, J.J. Heyd, E.N. Borhters, K.N. Kudin, V.N. Staroverov, T.A. Keith, R. Kobayashi, J. Normand, K. Raghavachari, A.P. Rendell, J.C. Burant, S.S. Iyengar, J. Tomasi, M. Cossi, J.M. Millam. M. Klene, C. Adamo, R. Cammi, J.W. Ochterski, R. L. Martin, K. Morokuma, O. Farkas, J.B. Forseman and D.J. Fox, Gaussian 16, Revision B.01, Gaussian, Inc., Wallingford CT (2016).
11. R. Dennington, T. Keith and J. Millam, Semichem Inc., Shawnee Mission, KS (2016).
12. A.D. Becke, *J. Chem. Phys.*, **98**, 5648 (1993); https://doi.org/10.1063/1.464913
13. C. Lee, W. Yang and R.G. Parr, *Phys. Rev. B Condens. Matter*, **37**, 785 (1988); https://doi.org/10.1103/PhysRevB.37.785
14. N. Singla and P. Chowdhury, *J. Mol. Struct.*, **1045**, 72 (2013); https://doi.org/10.1016/j.molstruc.2013.04.015
15. N.M. O'Boyle and J.G. Vos, GaussSum 3.0, Dublin City University (2005).
16. T. Lu and F. Chen, *J. Comput. Chem.*, **33**, 580 (2012); https://doi.org/10.1002/jcc.22885
17. W. Humphrey, A. Dalke and K. Schulten, *J. Mol. Graph.*, **14**, 33 (1996); https://doi.org/10.1016/0263-7855(96)00018-5
18. M.H. Jamróz, *Spectrochim. Acta A Mol. Biomol. Spectrosc.*, **114**, 220 (2013); https://doi.org/10.1016/j.saa.2013.05.096
19. P. Rajamani, V. Vijayakumar, N. Sundaraganesan, M. Jeeva and M.S. Boobalan, *Results Chem.*, **3**, 100096 (2021); https://doi.org/10.1016/j.rechem.2021.100096
20. V. Amir-Ebrahimi, A. Choplin, J. Demaison and G. Roussy, *J. Mol. Spectrosc.*, **89**, 42 (1981); https://doi.org/10.1016/0022-2852(81)90158-2
21. M. Sardari, F.K. Fotooh and M.R. Nateghi, *J. Mol. Model.*, **24**, 148 (2018); https://doi.org/10.1007/s00894-018-3667-y
22. C.Y. Panicker, K.R. Ambujakshan, H.T. Varghese, S. Mathew, S. Ganguli, A.K. Nanda and C.V. Alsenoy, *J. Raman Spectrosc.*, **40**, 527 (2009); https://doi.org/10.1002/jrs.2159
23. R. Arulraj, S. Sivakumar, S. Suresh and K. Anitha, *Spectrochim. Acta A Mol. Biomol. Spectrosc.*, **232**, 118166 (2020); https://doi.org/10.1016/j.saa.2020.118166
24. T.H.M. Nayaka, I. Pushpavathi, Pavithra and Y.R. Nagesh, *Russ. J. Bioorganic Chem.*, **50**, 211 (2024); https://doi.org/10.1134/S1068162024010229
25. L. Xiao-Hong, L. Xiang-Ru and Z. Xian-Zhou, *Comput. Theor. Chem.*, **969**, 27 (2011); https://doi.org/10.1016/j.comptc.2011.05.010
26. H. Singh, *Chem. Phys.*, **524**, 1 (2019); https://doi.org/10.1016/j.chemphys.2019.05.003
27. R.G. Pearson, *J. Org. Chem.*, **54**, 1423 (1989); https://doi.org/10.1021/jo00267a034
28. K. Fukui, T. Yonezawa and H. Shingu, *J. Chem. Phys.*, **20**, 722 (1952); https://doi.org/10.1063/1.1700523
29. A.P. Bandyopadhyay, A. Karmakar, J. Deb, U. Sarkar and M.M. Seikh, *Spectrochim. Acta A Mol. Biomol. Spectrosc.*, **228**, 117827 (2020); https://doi.org/10.1016/j.saa.2019.117827
30. Z. Liu, T. Lu and Q. Chen, *Carbon*, **165**, 461 (2020); https://doi.org/10.1016/j.carbon.2020.05.023
31. A.D. Isravel, J.K. Jeyaraj, S. Thangasamy and W.J. John, *Comput. Theor. Chem.*, **1202**, 113296 (2021); https://doi.org/10.1016/j.comptc.2021.113296
32. J. Poater, M. Duran, M. Solà and B. Silvi, *Chem. Rev.*, **105**, 3911 (2005); https://doi.org/10.1021/cr030085x

33. E. Matito, M. Duran and M. Solà, *J. Chem. Phys.*, **122**, 014109 (2005); https://doi.org/10.1063/1.2222352
34. T.M. Krygowski, *J. Chem. Inf. Comput. Sci.*, **33**, 70 (1993); https://doi.org/10.1021/ci00011a011
35. C.W. Bird, *Tetrahedron*, **41**, 1409 (1985); https://doi.org/10.1016/S0040-4020(01)96543-3
36. B. Donner, M. Kleber, C. Bracher and H.J. Kreuzer, *Am. J. Phys.*, **73**, 690 (2005); https://doi.org/10.1119/1.1930867
37. H.L. Schmider and A.D. Becke, *J. Mol. Struct. THEOCHEM.*, **527**, 51 (2000); https://doi.org/10.1016/S0166-1280(00)00477-2
38. M.R. Bozorgmehr, J. Chamani and G. Moslehi, *J. Biomol. Struct. Dyn.*, **33**, 1669 (2015); https://doi.org/10.1080/07391102.2014.967299
39. R.G. Parr and W. Yang, *J. Am. Chem. Soc.*, **106**, 4049 (1984); https://doi.org/10.1021/ja00326a036
40. A.O. Zacharias, A. Varghese, K.B. Akshaya, M.S. Savitha and L. George, *J. Mol. Struct.*, **1158**, 1 (2018); https://doi.org/10.1016/j.molstruc.2018.01.002
41. C. Morell, A. Grand and A. Toro-Labbé, *J. Phys. Chem. A*, **109**, 205 (2005); https://doi.org/10.1021/jp046577a
42. L.J. Bellamy, The Infrared Spectra of Complex Molecules, Chapman and Hall: London, U.K. (1975).
43. G. Socrates, Infrared and Raman Characteristics Group Frequencies, Wiley: New York, NY, USA, edn.: 3 (2001).
44. N. Sundaraganesan, H. Saleem, S. Mohan, M. Ramalingam and V. Sethuraman, *Spectrochim. Acta A Mol. Biomol. Spectrosc.*, **62**, 740 (2005); https://doi.org/10.1016/j.saa.2005.02.043
45. V. Krishnakumar and R. John Xavier, *Indian J. Pure Appl. Phys.*, **41**, 597 (2003).
46. V. Krishnakumar and N. Prabavathi, *Spectrochim. Acta A Mol. Biomol. Spectrosc.*, **71**, 449 (2008); https://doi.org/10.1016/j.saa.2007.12.033
47. A. Altun, K. Golcuk and M. Kumru, *J. Mol. Struct. THEOCHEM.*, **637**, 155 (2003); https://doi.org/10.1016/S0166-1280(03)00531-1
48. S.J. Singh and S.M. Pandey, *Indian J. Pure Appl. Phys.*, **12**, 300 (1974).
49. Y.X. Sun, Q.L. Hao, Z.X. Yu, W.J. Jiang, L.D. Lu and X. Wang, *Spectrochim. Acta A Mol. Biomol. Spectrosc.*, **73**, 892 (2009); https://doi.org/10.1016/j.saa.2009.04.012
50. N. Sundaraganesan, B.D. Joshua and T. Radjakoumar, *Indian J. Pure Appl. Phys.*, **47**, 248 (2009).
51. G. Shakila, S. Periandy and S. Ramalingam, *J. At. Mol. Opt. Phys.*, **2011**, 512841 (2011); https://doi.org/10.1155/2011/512841
52. V.R. Dani, Organic Spectroscopy, Tata-MacGraw Hill Publishing: New Delhi, India (1995).
53. A.R. Prabakaran and S. Mohan, *Indian J. Phys.*, **63B**, 468 (1989).
54. D. Vedal, O. Ellestad, P. Klaboe and G. Hagen, *Spectrochim. Acta A*, **32A**, 877 (1976); https://doi.org/10.1016/0584-8539(76)80159-6
55. N. Sundaraganesan, G. Elango, C. Meganathan, B. Karthikeyan and M. Kurt, *Mol. Simul.*, **35**, 705 (2009); https://doi.org/10.1080/08927020902873992
56. D. Sajan, J. Binoy, B. Pradeep, K.V. Krishna, V.B. Kartha, I.H. Joe and V.S. Jayakumar, *Spectrochim. Acta A Mol. Biomol. Spectrosc.*, **60**, 173 (2004); https://doi.org/10.1016/S1386-1425(03)00193-8
57. K. Furic, V. Mohacek, M. Bonifacic and I. Stefanic, *J. Mol. Struct.*, **267**, 39 (1992); https://doi.org/10.1016/0022-2860(92)87006-H
58. S. Sambandam, B. Sarangapani, S. Paramasivam and R. Chinnaiyan, *Biointerface Res. Appl. Chem.*, **11**, 11833 (2021); https://doi.org/10.33263/BRIAC114.1183311855
59. J.J. Kores, I.A. Danish, T. Sasitha, J.G. Stuart, E.J. Pushpam and J.W. Jebaraj, *Heliyon*, **7**, e08377 (2021); https://doi.org/10.1016/j.heliyon.2021.e08377
60. A.E. Reed, L.A. Curtiss and F. Weinhold, *Chem. Rev.*, **88**, 899 (1988); https://doi.org/10.1021/cr00088a005
61. M. Arivazhagan and R. Kavitha, *J. Mol. Struct.*, **1011**, 111 (2012); https://doi.org/10.1016/j.molstruc.2011.12.006
62. E. Kavitha, N. Sundaraganesan, S. Sebastian and M. Kurt, *Spectrochim. Acta A Mol. Biomol. Spectrosc.*, **77**, 612 (2010); https://doi.org/10.1016/j.saa.2010.06.034
63. L. Li, C. Wu, Z. Wang, L. Zhao, Z. Li, C. Sun and T. Sun, *Spectrochim. Acta A Mol. Biomol. Spectrosc.*, **136**, 338 (2015); https://doi.org/10.1016/j.saa.2014.08.153
64. D.A. Kleinman, *Phys. Rev.*, **126**, 1977 (1962); https://doi.org/10.1103/PhysRev.126.1977
65. K. Sambathkumar and G. Ravichandran, *Elixir Comput. Chem.*, **91**, 38077 (2016).
66. B. Rajasekhar, P.K. Muhammad Hijaz and T. Swu, *J. Mol. Struct.*, **1168**, 212 (2018); https://doi.org/10.1016/j.molstruc.2018.04.090
67. T. Sasitha and W.J. John, *Heliyon*, **7**, e06127 (2021); https://doi.org/10.1016/j.heliyon.2021.e06127
68. G.N. Ramachandran, C. Ramakrishnan and V. Sasisekharan, *J. Mol. Biol.*, **7**, 95 (1963); https://doi.org/10.1016/S0022-2836(63)80023-6